Environmental change in the Sea of Okhotsk during the last 1.1 million years

Dirk Nürnberg and Ralf Tiedemann
Leibniz Institut für Meereswissenschaften, Kiel, Germany

Received 2 March 2004; revised 9 July 2004; accepted 11 August 2004; published 3 November 2004.

[1] On the basis of two sedimentary records from the central Sea of Okhotsk, we reconstruct the closely coupled glacial/interglacial changes in terrigenous flux, marine productivity, and sea ice coverage over the past 1.1 Myr. The correspondance of our sedimentary records to the China loess grain size record (China loess particle timescale, CHILOPARTS) suggests that environmental changes in both the Sea of Okhotsk area and in SE Asia were closely related via the Siberian atmospheric high-pressure cell. During full glacial times our records point to a strong Siberian High causing northerly wind directions, the extension of the sea ice cover, and a reduced Amur River discharge. Deglacial maxima of terrigenous flux were succeeded by or synchronous to high-productivity events. Marine productivity was strengthened during glacial terminations because of an effective nutrient utilization at times of enhanced water column stratification and high nutrient supply from fluvial runoff and sea ice thawing. During interglacials, SE monsoonal winds prevailed, analogous to today's summer situation of a pronounced Mongolian Heat Low and a strong Hawaiian High. Strong freshwater discharge induced by high precipitation rates in the Amur drainage area and a seasonally reduced and mobile sea ice cover favored marine productivity (although being considerably lower than during the terminations) and a lowered flux of ice-rafted detritus. *INDEX TERMS:* 1620 Global Change: Climate dynamics (3309); 3344 Meteorology and Atmospheric Dynamics: Paleoclimatology; 4267 Oceanography: General: Paleoceanography; 9355 Information Related to Geographic Region: Pacific Ocean; 9604 Information Related to Geologic Time: Cenozoic; *KEYWORDS:* Sea of Okhotsk, paleoproductivity, terrigenous flux, sea ice dynamics, stratigraphy

Citation: Nürnberg, D., and R. Tiedemann (2004), Environmental change in the Sea of Okhotsk during the last 1.1 million years, *Paleoceanography*, *19*, PA4011, doi:10.1029/2004PA001023.

1. Introduction

[2] Bound by the Asian continent to the northwest and north and the Kurile-Kamchatka-Island Arc to the east and southeast, the Sea of Okhotsk is the second largest marginal sea of the Pacific (Figure 1). Despite its significant role for the modern hydrology of the NW Pacific, its high primary productivity, and its pronounced seasonality in sea ice coverage, it still is one of the paleoceanographically less studied ocean basins. In view of strengthened efforts of better understanding cool climate dynamics, the Sea of Okhotsk became an increasing focus of interest. The area is regarded as a relic of the last glacial, because its modern seasonal sea ice cover extends south as far as 43°N. The highly dynamic sea ice coverage largely affects the sedimentation patterns. During summer, the ice-free conditions favor a high biotic activity changing the Sea of Okhotsk into an extremely high-productivity area. During autumn and winter, extensive brine rejection caused by sea ice formation leads to the formation of Sea of Okhotsk Intermediate Water (SOIW), which effectively ventilates the NW Pacific.

[3] Marine geological studies in the Sea of Okhotsk started in the 1950s and 1960s by *Bezrukov* [1955, 1960], *Lisitzin* [1951, 1974], *Jouse and Koreneva* [1959], and *Jouse* [1962]. These studies showed that during interglacial times, sediments enriched in biogenic silica, calcium carbonate, and organic carbon accumulated while during glacial times terrigenous material dominated. Unfortunately, the time control of these studies was not yet validated, and the correlation to marine isotope stages (MIS) was not existent. *Gorbarenko et al.* [2000a, 2000b, 2002] were the first to establish a stratigraphical framework for the Sea of Okhotsk over the last ~120.000 years based on AMS ^{14}C dating, oxygen isotope stratigraphy, and tephrachronology.

[4] From these studies and from our own initiatives within the framework of the joint German/Russian project KOMEX [*Nürnberg et al.*, 1997b; *Biebow and Hütten*, 1999; *Biebow et al.*, 2003], the paleoceanographic potential of this NW Pacific marginal basin became apparent: (1) The carbonate-containing sediments permitted establishment of a continuous high-resolution oxygen isotope stratigraphy, which is very rare in the Subarctic-Pacific area typically characterized by large water depths and a shallow lysocline. (2) The marine deposits facilitate insights into the closely coupled interplay between high surface productivity, terrigenous supply and sea ice coverage. This is of specific interest, since the interglacial high productivity in the North Pacific and its marginal seas act as a sink of CO_2 that may counteract to the naturally induced atmospheric CO_2 increase during deglaciations and subsequent interglacials.

0883-8305/04/2004PA001023

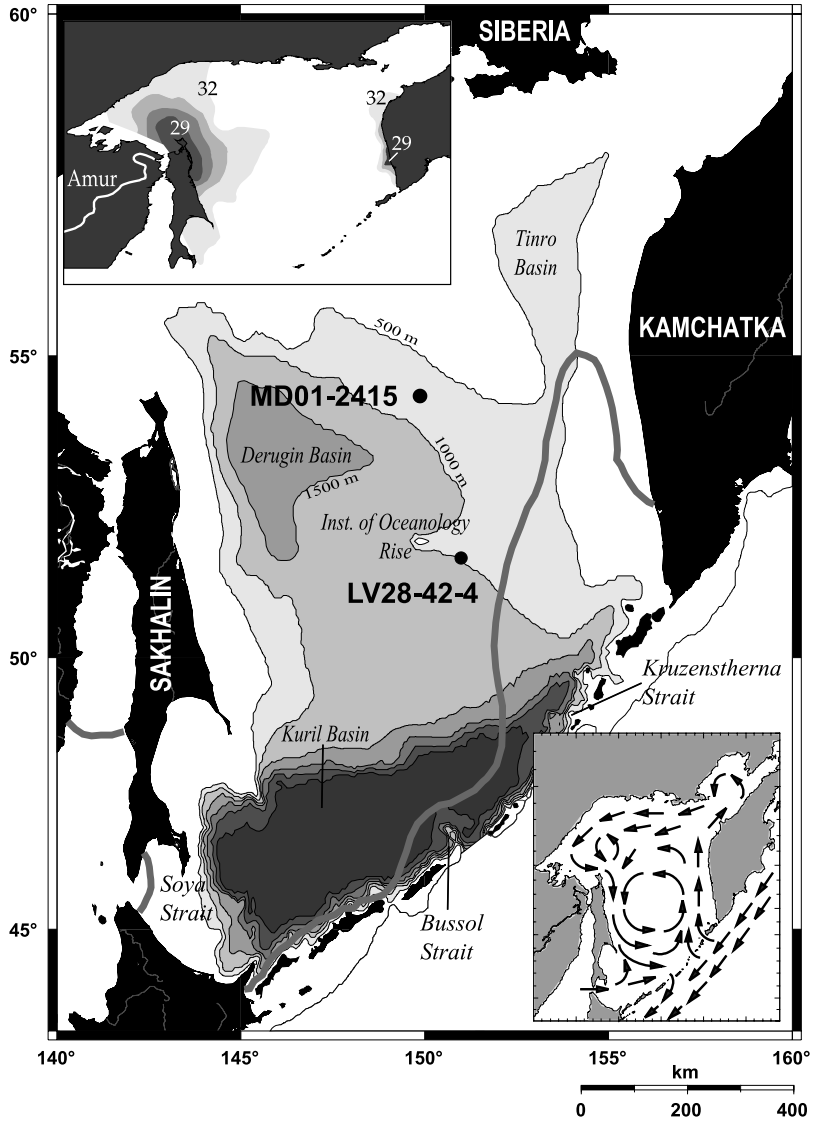

Figure 1. Bathymetric chart of the study area showing core locations. Core MD01-2415 was recovered from a narrow stripe of international waters within the Sea of Okhotsk. Thick line indicates the sea ice concentration >25% during March 1980 (NASA, Nimbus 7). Inset in top left corner shows sea surface salinities (September–October 1999) from *Kitani* [1973]. Inset in bottom right corner shows general cyclonic surface circulation pattern.

[5] In this study, we present two sediment records from the central part of the Sea of Okhotsk, which extend the existing paleoceanographic data sets back to ~1.1 Myr, and allow us to decipher the long-term environmental change over several glacial/interglacial cycles back to MIS 32. The sedimentological, geochemical and geophysical data sets reveal a complex interplay between fluvial supply, sea ice transport, marine productivity, and atmospheric circulation.

2. Modern Oceanographic and Climatic Variability

[6] The surface hydrography of the Sea of Okhotsk is characterized by a large cyclonal gyre, which is mainly driven by the inflow of relatively warm and saline Pacific water masses through Kruzenstherna Strait. This Kamchatka Current flows along western Kamchatka and mixes with water masses from the broad northern shelf areas [*Alfutis and Martin*, 1987]. In prolongation, the East Sakhalin Current flows along Sakhalin southward toward the Kurile Islands and leaves the Sea of Okhotsk through Bussol Strait. In addition, saline surface water masses intrude from the Sea of Japan through Soya Strait.

[7] The Sea of Ohkotsk plays an important role for the formation and ventilation of North Pacific Intermediate Water (NPIW) [*Ohtani and Nagata*, 1990; *Riser*, 1990; *Talley*, 1991; *Freeland et al.*, 1998; *Martin and Kawase*, 1998; *Wong et al.*, 1998; *Winckler et al.*, 1999]. Winter sea ice on the northern and western shelves causes intensive formation of SOIW. The oxygenated SOIW spreads across

the Sea of Okhotsk in depths of 200–1000 m according to its potential density of max. 27.4 [*Wong et al.*, 1998]. It leaves the Sea of Okhotsk at a rate of ~2.7 Sv and ventilates the intermediate water depths of the North Pacific.

[8] Below the SOIW, old, CO_2-enriched and carbonate-aggressive deep Pacific water masses intrude predominantly via Krusenstherna Strait, which is ~1900 m deep. Outflow of deep water masses mainly takes place through Bussol Strait (2300 m deep). The interface between the Pacific deep waters and the overlying SOIW is defining the depth of the lysocline.

[9] The climate of the Sea of Okhotsk area is influenced by the adjacent NE Siberian landmasses. The strong temperature gradient between summer (18°C) and winter (−32°C) [*Wakatsuchi and Martin*, 1990] indicates a polar, continental climatic regime. During winter, a strong atmospheric Siberian High interacts with the Aleutian Low resulting in strong and cold northerly winds, which affect sea surface temperatures (SST) and sea ice coverage in the Sea of Okhotsk [*Parkinson*, 1990; *Tchaibana et al.*, 1996; *Ponomorev et al.*, 1999]. Decadal variations in strength and location of these atmospheric action centers covary with the Arctic Oscillation (AO) [*Overland et al.*, 1999], but also with the Pacific Decadal Oscillation (PDO) [*Mantua et al.*, 1997]. The Arctic Oscillation is suggested to form the major climate forcing mechanism of the high-latitude Northern Hemisphere [*Wallace*, 2000]. The PDO, instead, is a prominent ocean-atmosphere teleconnection pattern that links El Niño Southern Oscillation (ENSO)-driven changes in tropical SST with meteorological and oceanic changes in the North Pacific [*Trenberth and Hurrell*, 1994]. This oscillation paces with periodicities of 15–25 and 50–70 years [*Mantua et al.*, 1997; *Minobe*, 1999] and tends to be positive during El Niño warm events. During such events, the strengthened Aleutian Low enhances advection of cold air masses from NE Siberia and creates cool SST in the western North Pacific [*Trenberth et al.*, 1998]. Changes in Sea of Okhotsk sea ice cover and SST pace at similar periods of about 7–10, 18–25, and 50 years [*Cavalieri and Parkinson*, 1987; *Ustinova et al.*, 2000], and point to the possibility of tropical forcing on Sea of Okhotsk winter sea ice dynamics [*Tchaibana and Wakahama*, 1989; *Ponomorev et al.*, 1999].

[10] The summer situation differs considerably from the winter scenario, and is typically characterized by the close interrelationship between the South Asian Low and the North Pacific (Hawaiian) High atmospheric action centers [*Wang and Li*, 1990]. Caused by strong surface heating over the semiarid regions of northern China and the Mongolian Plateau, the heat low of the Asian monsoon extends to northern Mongolia [*Miyazaki and Yasunari*, 1999]. Enhanced precipitation in the Amur River drainage area (1.85×10^6 km^2 [*McLennan*, 1995]) affects the river discharge to the Sea of Okhotsk during summer.

[11] The Amur River entering the northern Sea of Okhotsk has a sediment runoff, which is 2–3 times higher (~14 t km^{-2} year^{-1} [*Anikiev et al.*, 2001]) than all other large Siberian rivers, including those draining into the Arctic Ocean. Significant freshwater discharge, coupled with the extraordinarily high suspension freight [*Ogi et al.*, 1995], occurs from May until October (~0.02 km^3/s), while the Amur is frozen from November to April. A first peak in fluvial discharge is observed in June mainly attributed to melting of snow and frozen soil. A second, larger peak during September reflects the preceding monsoonal precipitation maximum (July, August) in the Amur drainage area. The main pathway of fluvial discharge around the northern tip of Sakhalin and along the eastern continental margin of Sakhalin is reflected by both a pronounced anomaly in sea surface salinity (<32.5 [*Kitani*, 1973]) (Figure 1), and by a surface layer of high turbidity as seen from satellite imagery (http://seawifs.gsfc.nasa.gov/SEAWIFS.html). The freshwater supply contributes to a strong stratification of near-surface water masses, and causes the formation of the dichothermal layer during summer (50–150 m water depth [*Freeland et al.*, 1998].

[12] Both, atmospheric circulation pattern and fluvial discharge effectively shape the spatial and temporal occurrence of sea ice in the Sea of Okhotsk. Sea ice extent advances by wind-driven ice advection, and daily scale variation in ice extent is controlled by wind speed [*Kimura and Wakatsuchi*, 2001]. Coastal polynyas on the northwestern shelves and at Kashevarov Bank [*Alfutis and Martin*, 1987] enhance sea ice formation.

[13] Fluvial discharge also shapes sea ice formation, although views on mechanistic coherencies deviate. *Rostov and Zhabin* [1991] suggested that sea surface freshening promotes winter freezing, whereas *Ogi et al.* [2001] stated that the fluvial freshwater discharge causes a thermal anomaly in the northwestern Sea of Okhotsk suppressing sea ice formation in the succeeding winter. Summer-induced reductions in the buildup of winter sea ice may in turn affect atmospheric processes, because heat and moisture fluxes from the sea surface are being favored and consequently, warm the atmosphere above the sea ice cover.

[14] Main freeze-up starts during November in the northern Sea of Okhotsk, and maximum sea ice extent is reached during March. On average, 80% of the Sea of Okhotsk are ice covered during that period [*Wadachi*, 1987], with ice thicknesses of 0.5–1 m [*Aota and Uematsu*, 1989]. The seasonal sea ice cover is highly dynamic, and shows a decadal variability [*Parkinson and Gratz*, 1983; *Cavalieri and Parkinson*, 1987].

[15] Primary productivity in the Sea of Okhotsk is extremely high, caused by a complex interplay of seasonal changes in sea ice coverage, fluvial discharge, meltwater supply, and intruding surface water masses from the Pacific Ocean and Sea of Japan. Highest marine productivity occurs during summer, and is mainly caused by siliceous plankton (diatoms) [*Koblentz-Mishke et al.*, 1970]. Color ocean charts from NASA (SEAWIFS Project] indicate chlorophyll-a concentrations of up to 50 mg/m^3, which compare to other high-productivity areas on Earth. Plankton blooms occur twice a year. The spring bloom coincides with sea ice melting, whereas the autumn bloom starts with the onset of sea surface cooling. Plankton blooms are restricted to the upper 30–50 m [*Zenkevitch*, 1963]. The formation of the dichothermal layer during summer favors bioproductivitiy

Table 1. Site Information

Core	Latitude, °N	Longitude, °E	Depth, mbsl	Recovery, m
LV28-42-4	51°42.89′	150°59.13′	1041	10.84
MD01-2415	53°57.09′	149°57.52′	822	46.23

due to the high-nutrient utilization efficiency [*Talley and Nagata*, 1995].

3. Materials and Methods

3.1. Core Selection

[16] The study focuses on two sediment records from central parts of the Sea of Okhotsk (Figure 1 and Table 1). The selection of core locations was based on extensive previous sedimentological and sediment-echo sounding studies. Gravity core LV28-42-4 (51°42.89N 150°59.13E) was recovered from 1041 m water depth during LV28 cruise with RV *Akademik Lavrentiev* in 1998 [*Biebow and Hütten*, 1999]. Approximately 140 nautical miles further to the north, we recovered the CALYPSO giant piston core MD01-2415 (53°57.09N 149°57.52E) from 822 m water depth during cruise WEPAMA with the French RV *Marion Dufrèsne* [*Holbourn et al.*, 2002]. Both sites are bathed in North Pacific Water masses (NPW). Sediments at both core locations are quite similar. Greenish-gray to dark gray terrigenous silts dominate, containing varying quantities of clay, sand, and pebbles. The monotonous, bioturbated terrigenous sequences are repeatedly interrupted by thin layers of light olive-gray diatomaceous oozes of silty sand to clayey silt, showing biogenic opal concentrations of up to 50%. The detailed description of the lithologies of both cores is given by *Biebow and Hütten* [1999] and *Holbourn et al.* [2002].

3.2. Methods

3.2.1. Stratigraphic Approach

[17] The chronostratigraphic framework of cores LV28-42-4 and MD01-2415 is based on a combination of stable oxygen isotope stratigraphy, AMS ^{14}C dating, and orbital tuning. Stable oxygen and carbon isotope measurements were made on 2–3 specimens of the endobenthic foraminiferal species *Uvigerina auberiana*, and *Uvigerina akitaensis* (*Uvigerina peregrina* of authors) from the 250–500 μm size fraction. We did not observe any interspecies offset in the δ^{18}O signal. The size fraction 250–500 μm was chosen to eliminate redeposited tests of smaller specimens that may cause a bias of the benthic isotope signal [*Lutze et al.*, 1979]. According to *Shackleton and Hall* [1984], *Uvigerina* δ^{18}O values appear to be in equilibrium with seawater δ^{18}O.

[18] All foraminiferal tests were ultrasonically cleaned in distilled water prior to analyses. The isotopic analyses were performed at GEOMAR on a Finnigan MAT 252 mass spectrometer with an automated Kiel carbonate preparation line. The mass spectrometers are calibrated to NBS 19 (National Bureau of Standards), and the isotope values are reported on the VPDB (Vienna PDB) scale. The external reproducibility of in-house carbonate standards was ±0.03‰ for δ^{18}O and 0.01‰ for δ^{13}C (1σ values).

[19] Accelerator mass spectrometry radiocarbon dating (AMS ^{14}C) in the uppermost core sections of core LV28-42-4 provided additional stratigraphical information (Table 2). Analyses were conducted at the Leibniz Laboratory for Radiometric Dating and Isotope Research at Kiel. Measurements were performed on the planktonic foraminifer *Neogloboquadrina pachyderma* sin. from the 125–250 μm fraction. Conversion to calendar ages was accomplished using the Calib 4.1.2 calibration program [*Stuiver and Reimer*, 1993] after applying a reservoir correction of 1000 years for planktonic ^{14}C ages according to *Southon et al.* [1990], *Gorbarenko et al.* [2000a, 2000b], and *Yoneda et al.* [2000].

[20] The chronostratigraphy is based on the graphic correlation of the benthic oxygen isotope curves with the stacked standard record of *Bassinot et al.* [1994] and *Mix et al.* [1995]. The marine oxygen isotope events (MIS) were identified following the standard δ^{18}O nomenclature proposed by *Prell et al.* [1986] and *Tiedemann et al.* [1994]. Figure 2 presents the stratigraphical framework of core LV28-42-4 covering the last 350 ka. The age control of the last ~11 kyr relies on AMS ^{14}C dating. The interval from 11 ka to 350 ka is solely based on benthic δ^{18}O stratigraphy. Accordingly, the benthic δ^{18}O record reveals a strong response to cyclic fluctuations in Earth's orbital parameters of eccentricity (100 kyr), obliquity (41 kyr) and precession (23 and 19 kyr).

[21] For core MD01-2415, the stratigraphic interpretation of the benthic δ^{18}O signal was difficult, because benthic foraminifers are generally rare and partly absent in some core intervals. Fortunately, the astronomical calibration of the timescale [e.g., *Tiedemann et al.*, 1994; *Tiedemann and Haug*, 1995] became feasible, as the core is characterized by high-frequency cyclic variations in various sediment properties. Here, we used the shipboard color b* value [*Holbourn et al.*, 2002] as a tuning medium, which is

Table 2. AMS ^{14}C Dating in Core LV28-42-4[a]

Depth, cm	^{14}C Age, years B.P.	Standard Deviation, years	Reservoir Corrected ^{14}C Age, years B.P.	±1 σ, years	Calendar Age, years	Laboratory Number
3–4	3330	70	2330	2331–2531	2396	KIA 9152
33–34	4425	40	3425	3698–3825	3771	KIA 9154
44–45	4955	40	3955	4418–4524	4492	KIA 9155
85–86	11375	60	10,375	11,730–12,340	12,092	KIA 9156

[a]Dated material is planktonic foraminiferal tests (1000–2000 specimens of *N. pachyderma* sin.). Raw AMS ^{14}C ages were converted into calendar years according to the work of *Stuiver and Reimer* [1993].

indicative of cyclic changes in biogenic silica production (see below). The average sample spacing for b* measurements is 2 cm. The first step toward astronomical calibration was to examine the cyclic variations of the b* record in the depth domain (Figure 3). The frequency spectrum of the b* values is marked by a pronounced cycle of 1.32 m. Using age control points initially derived from the oxygen isotope stratigraphy, we found a good match in cyclicity and amplitude fluctuations between orbital precession and the 1.32 m filter output (Figure 4). The precession-related filter

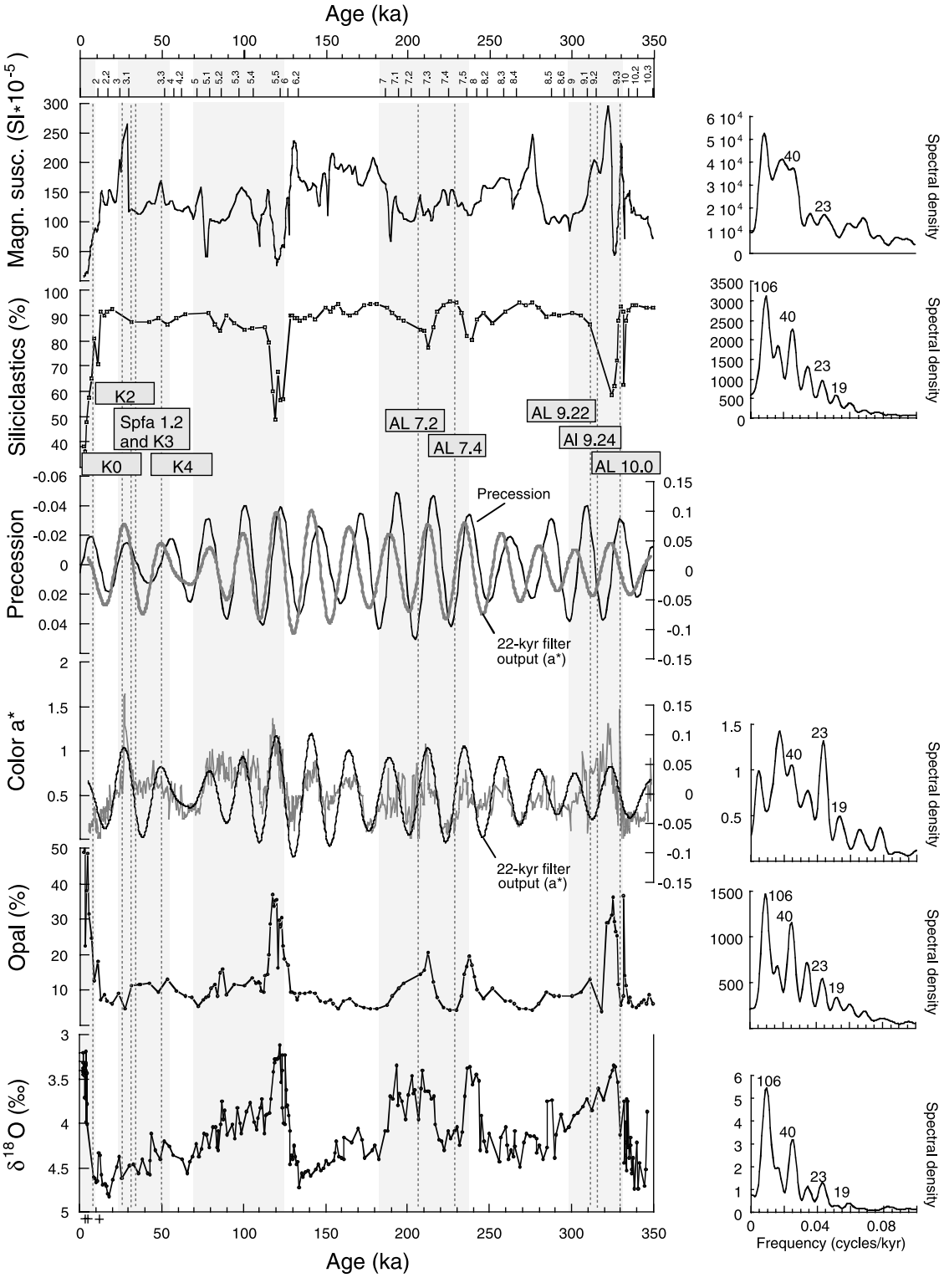

Figure 2

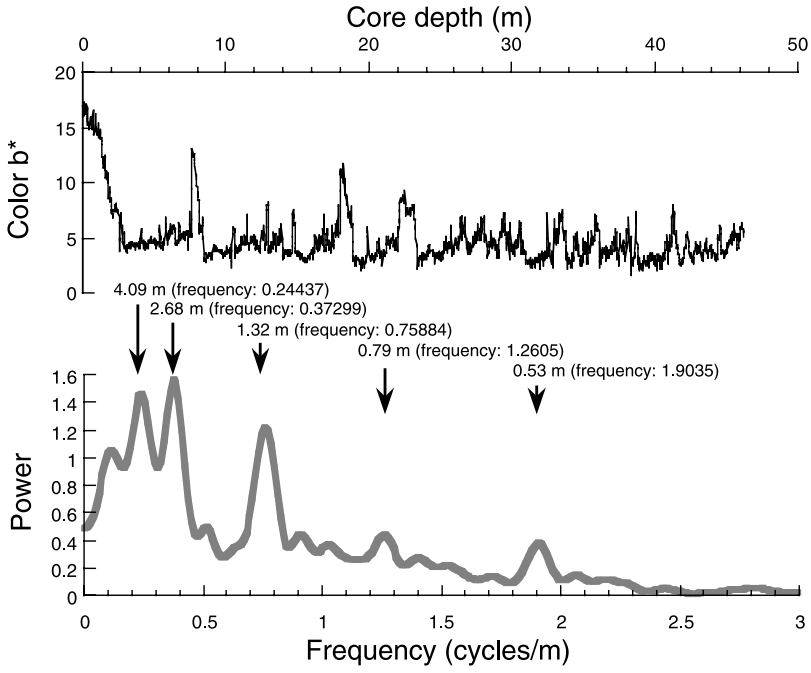

Figure 3. Color b* variations of core MD01-2415 versus core depth and according frequency spectrum of color b* variations in the depth domain. The cycle with a prominent wavelength of 1.32 m is related to orbital forcing of precession.

output was then used to generate a timescale that brings the filtered cycles in phase with the inferred astronomical forcing. Color b* value maxima were tuned to Northern Hemisphere (June) insolation maxima assuming a phase difference of 5 kyr. As a result, this tuning brought the $\delta^{18}O$ record of core MD01-2415 in phase with the $\delta^{18}O$ standard record of *Mix et al.* [1995].

[22] After tuning, the color b* record was finally filtered in the time domain at the main orbital frequencies. The amplitude variations of orbital precession and the 22 kyr filter output are remarkably similar, suggesting that we correctly mapped the climate signal onto the astronomical record (Figure 4). The 41 kyr filter output appears to be in phase with orbital obliquity. Figure 4 exhibits the final stratigraphy of core MD01-2415, which composes the time interval of the last 1.1 Myr.

3.2.2. Calculation of Sedimentation Rates and Quantification of Flux Rates

[23] Sedimentation rates (in cm kyr^{-1}) were calculated by dividing the thickness of sediment intervals between age control points by their duration of deposition (Figure 5). Sedimentation rates were generally low at both sites, and vary from $\sim$2–4 cm kyr^{-1} for most of the time studied. Core LV28-42-4 generally shows lower sedimentation rates. Only during pronounced interglacial times, sedimentation rates significantly increased, reaching maximum values of >20 cm kyr^{-1} during the Holocene.

[24] The calculation of proxy accumulation rates depends on a reliable chronostratigraphic framework and on the accurate assessment of dry bulk densities of sediments [*Van Andel et al.*, 1975]. Measurements of dry bulk densities were performed each 5 cm for core LV28-42-4, and each 10 cm for core MD01-2415. Bulk accumulation rates range between $\sim$1–7 g cm^{-2} kyr^{-1}, with in average lower values at Site LV28-42-4. Maximum accumulation rates appear during interglacial times and during terminations. Extremely high bulk accumulation rates of >15 g cm^{-2} kyr^{-1} by far exceeding all other maxima are observed at both sites during the Holocene. The core top bulk accumulation rate at site location MD01-2415 is

Figure 2. The age model of core LV28-42-4 is based on benthic oxygen isotope stratigraphy (for comparison, see reference isotope stack of *Bassinot et al.* [1994]), supported by AMS ^{14}C dating in the uppermost core section (crosses along timescale). The frequency spectra of the different proxy data (right) indicate dominant cyclicities of 100 kyr, 41 kyr, 23 kyr, and 19 kyr as a response to cyclic fluctuations in the Earth's orbital parameters eccentricity, obliquity and precession. The 22 kyr filter output of the a* color spectrum matches the orbital precession. The precessional filter has a central frequency of 0.047 cycles/kyr and bandwidth of 0.01 cycles/kyr. The comparison of typical structures between siliciclastics, magnetic susceptibility, opal records, the frequent occurrence of volcanic ash layers (shaded lines and shaded boxes; nomenclature according to *Gorbarenko et al.* [2002] and *Kaiser* [2000]), and the dominant 22 kyr cyclicity in the red-green color spectrum (a*) of the sediments allows detailed correlation of sediment records across the Sea of Okhotsk and thus a transfer of age control points. Shaded areas indicate interglacial periods.

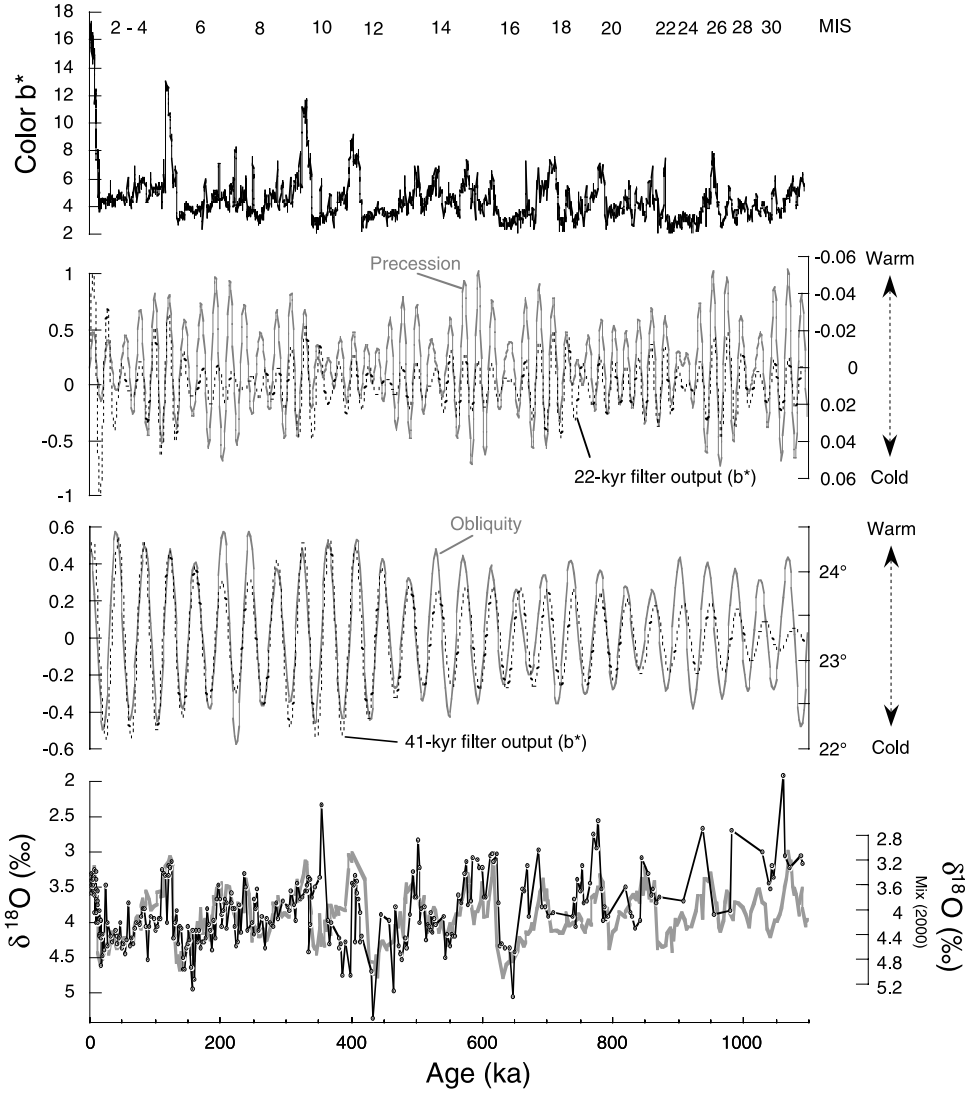

Figure 4. Stratigraphical framework of core MD01-2415 showing the benthic oxygen isotope record (bottom curve, dots) underlain by the oxygen isotope reference record of *Mix et al.* [1995] of ODP Site 849. The sediment color b* record (top curve) is applied to astronomically calibrate the timescale. The filtered 22 kyr and 41 kyr components of color b* values (shaded curves) are compared with orbital precession and obliquity. The precessional (obliquity) filter has a central frequency of 0.047 (0.025) cycles/kyr and a bandwidth of 0.01 (0.003) cycles/kyr. Numbers delineate marine oxygen isotope stages.

$\sim$19 g cm^{-2} kyr^{-1}. At site LV28-42-4, it amounts to $\sim$15 g cm^{-2} kyr^{-1}. It may be argued that these extreme values are artifacts due to the coring techniques applied. Recently, *Skinner and McCave* [2003] stated that heavier piston corers deployed on longer, lighter cables (in particular the CALYPSO device applied here), are prone to greater oversampling ratios over longer stratigraphic intervals. For the CALYPSO giant piston core MD01-2415, under pressuring and piston suction during core retrieval is most likely to have happened, probably generating the high sedimentation and accumulation rates observed during Termination I and the Holocene period. Sediment distortion and outflow during deck handling, in turn, might have been responsible for sediment thinning of the youngest sediments in core LV28-42-4. A more reliable estimate comes from undisturbed multicorer records from adjacent site locations [*Kaiser*, 2000], which suggests $\sim$9 g cm^{-2} kyr^{-1} of bulk accumulation at Site LV28-42, implying that CALYPSO coring may lead to an overestimation of core top bulk accumulation rates.

3.2.3. Reconstruction of Paleo-export Production

[25] To assess changes in paleoproductivity (here: paleo-export production), a suite of proxy parameters (total organic carbon, calcium carbonate, biogenic silica, excess barium, and chlorins) was gathered. Diatomaceous oozes are widespread in the Sea of Okhotsk, pointing to siliceous plankton being the main primary producer. To quantify the concentrations of biogenic silica (opal), we applied an automated leaching method according to *Müller and Schneider* [1993] (e.g., Figure 2). The opaline material is extracted from the dry and ground bulk sediment by

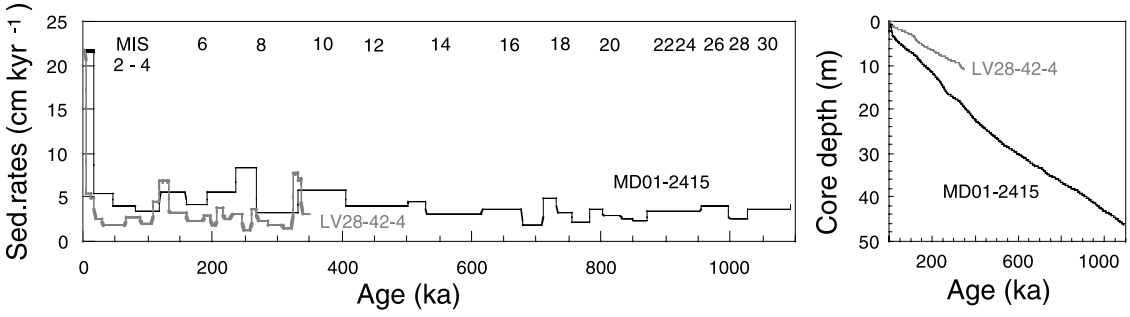

Figure 5. (left) Sedimentation rates of cores LV28-42-4 and MD01-2415 versus age and (right) according depth versus age diagram. Sedimentation rates commonly vary between 2 and 4 cm/kyr, except during pronounced deglacial phases when sedimentation rates increase to even >20 cm/kyr.

sodiumhydroxide at ~85°C for ~45 min. The leaching solution is continuously analyzed for dissolved silicon by molybdate-blue spectrophotometry. The *DeMaster* [1981] mineral correction was consequently applied.

[26] Chlorin concentrations in deep-sea sediments are considered to reflect variations in primary surface ocean productivity [e.g., *Harris et al.*, 1996], as terrestrially derived chlorophyll rapidly deteriorates and commonly does not contribute to the chlorin concentrations measured in the pelagic realm. To determine chlorins, which include a whole suite of degradation products of chlorophyll, freeze-dried subsamples were extracted by threefold sonication and centrifugation in acetone. Sediment extracts were measured fluorometrically (TD-700 fluorometer) immediately after extraction.

[27] Total carbon contents of sediment samples were determined with a CARLO ERBA Model NA 1500 CNS analyzer. Total carbon (TC) was derived from bulk sediments, whereas total organic carbon (TOC) content was measured on decalcified sediment samples. The inorganic carbon content (IC) was calculated as the difference between TC and TOC, i.e., IC = (TC-TOC) × 8.333. In order to assess terrigenous sources of TOC, atomic organic carbon *versus* total nitrogen ratios ([C/N]a) were calculated. Typically, marine organic matter exhibits [C/N]a ratios of 5–8 close to the Redfield ratio of marine phytoplankton ([C/N]a ~ 7) [*Redfield et al.*, 1963], while terrestrially derived organic matter has ratios between 25 and 35 [*Emerson and Hedges*, 1988].

[28] Sedimentary barite is commonly used as a proxy for paleoproductivity [e.g., *Shimmield et al.*, 1994], although the process by which barite forms is still not known sufficiently. It most presumably is closely coupled to the silica cycle in the oceans. Barium, and also the typically terrestrial elements aluminum, titanium, and iron, were measured in bulk sediment on a sequential wavelength-dispersive Phillipps PW1400 X-ray fluorescence spectrometer according to standard procedures. In order to calculate the biogenically derived portion of barium (Ba_{excess}), total barium was corrected for the nonbiogenic portion [e.g., *Nürnberg et al.*, 1997a]. Export production (P_{new}) was assessed from Ba_{excess} using the equation of *Nürnberg* [1995], as TOC includes a major terrigenous component (see below).

3.2.4. Assessment of Terrigenous Supply

[29] The impact of terrigenous flux was assessed from geochemical proxy data (i.e., concentrations of titanium, aluminum, iron) in combination with sedimentological (percentages of siliciclastics, fine fraction) and shipboard magnetic susceptibility data. The magnetic susceptibility was measured immediately after retrievel of the sediment cores with a Bartington Loop sensor (MS2C) in conjunction with a control unit (MS2) for core LV28-42-4 [*Biebow and Hütten*, 1999], and with the GEOTEK core logging system for core MD01-2415 [*Holbourn et al.*, 2002]. Commonly, magnetic susceptibility is inversely correlated to color b* values, and matches the >63 μm record (in percent of bulk sediment), hence approximating variations in terrigenous material. In fact, magnetic susceptibility and percentages of the <63 μm fraction would even better correlate if the portions of opal and $CaCO_3$ in the fine fraction could be estimated. As $CaCO_3$ is preponderantly provided by coarse foraminiferal calcite, mainly opal contributes to the fine fraction.

[30] To assess the percentage of terrigenous material more accurately, we pursued two approaches. First, we normalized the aluminum and titanium concentrations to the average Russian Paleozoic shale aluminum (3313 μmol g^{-1}) and titanium concentrations (115.2 μmol g^{-1}) [*Ronov and Migdisov*, 1971]. The aluminum value corresponds to the "North American shale composite" of 3315 μmol g^{-1} [*Gromet et al.*, 1984]. The titanium value is close to the average upper continental crust titanium value of 110.7 μmol g^{-1} [*Taylor and McLennan*, 1985]. Second, percentages of siliciclastic (terrigenous) material were calculated by subtracting % opal, % $CaCO_3$ and % TOC from bulk sediment. The resulting records match the magnetic susceptibility records. Both approaches to assess the terrigenous portion produce the same downcore trends.

[31] Ice rafting is a major transport process for large quantities of siliciclastic material. The identification of ice-rafted debris (IRD) is critical, and various approaches are commonly used. Here, we define the 125–500 μm fraction as IRD. In order to avoid bias from calcareous and siliceous plankton in this fraction specifically during warm periods, we related the percentages of the 125–500 μm fraction to the siliciclastic fraction. For core LV28-42-4, IRD was further assessed by calculating grain

percentages of major lithogenic components (quartz, rock fragments, feldspar, dark minerals) in the 125–500 μm fraction. Both approaches led to comparable results.

[32] All analytical data presented are available through the World Data Center-A for Paleoclimatology.[1]

4. Results and Discussion

4.1. Supply of Terrigenous Material

4.1.1. Identification

[33] Sedimentation in the Sea of Okhotsk is dominated by terrigenous (siliciclastic) material. Both cores reveal similar patterns of temporal variability in proxy data, and the various parameters resemble each other in concentration (Figure 6). The monotonous terrigeneous sequences, characterized by >85% siliciclastics, magnetic susceptibilities of 100–250 SI $\times$ 10^{-5} and low b* values, are only interrupted by short, interglacial/interstadial events of extremely enhanced paleoproductivity. During these periods, the siliciclastic portion declines to even below 35%. At both sites studied, the terrigenous (siliciclastic) portion is mainly bound to the silt and clay fractions, which commonly have concentrations >65% throughout the time interval studied. Concentrations of siliciclastics and the fine fraction (<63 μm) resemble each other in both cores.

[34] Most characteristic for the Sea of Okhotsk sediments is the common basin-wide and temporally continuous abundance of ice-rafted debris (Figure 6). Dropstones of 3–5 cm size are present in both cores, and are predominantly well rounded. The 125–500 μm fraction is considered to reflect ice rafting at best. In both cores, the downcore variability of the 125–500 μm fraction is similar, although the percentages of the 125–500 μm fraction are consistently higher by ~8% in average in core LV28-42-4 than in the more northern core MD01-2415 over the last ~350 kyr. Also, the amplitude variations are more pronounced in core LV28-42-4. The percentages of the lithogenic components (quartz, rock fragments, mica, dark minerals) range between 0–80%, and generally match the temporal variations of the 125–500 μm fraction.

[35] In core MD01-2415, a subtle change to lower portions of IRD is visible at ~600–400 ka, in line with a general fining in grain size (Figure 6). Prior to ~600–400 ka, maxima in magnetic susceptibility were controlled by maxima in IRD content as both records are well (positively) correlated. During the last ~400 ka, the correlation between IRD and magnetic susceptibility significantly weakened, while the (although negative) correlation between magnetic suceptibility and fine fraction (<63 μm) became dominant.

4.1.2. Source

[36] The geochemical approach helped us to further characterize type and source of terrigenous matter. For core LV28-42-4, we observe a good correlation between aluminum and titanium (r = >0.98), between titanium and iron (r = >0.97), and between aluminum and iron (r = >0.95) suggesting that these elements share a common terrigenous source.

[37] Titanium concentrations correlate to the percentages of siliciclastic material (r = 0.95), supporting the terrigenous origin of these elements. This is important because the percentage of siliciclastic material was determined independently from metal records, and thus corroborates the chemical analyses. Both, $Al_{normalized}$ and $Ti_{normalized}$ show clear glacial/interglacial variability with elemental concentrations higher during glacials, and significantly lower during interglacials.

[38] As different rock types have different Al/Ti ratios [*Taylor and McLennan*, 1985], the Al/Ti ratio was used to identify source types of detrital material. The Al/Ti record of core LV28-42-4 exhibits an overall range of ~23–45 (mol/mol) over the last ~350 kyr (Table 3). The mean Al/Ti ratio of ~36 (mol/mol) ±3 standard deviation corresponds to core top Al/Ti ratios of 35–41 from the deep central Sea of Okhotsk (Nürnberg, unpublished data, 2004), and is close to the North American shale composite (~34 [*Gromet et al.*, 1984]) and to average pelagic clay (~32 [*McLennan*, 1995]), but clearly lower than Russian Paleozoic shale (~28 [*Ronov and Migdisov*, 1971]). Loess deposits exhibit similarly high Al/Ti molar ratios of ~30–34 [*Taylor et al.*, 1983; *McLennan*, 1995]. The average continental crust has an Al/Ti molar ratio of >40 [*Taylor and McLennan*, 1981; *McLennan*, 1995]. Oceanic basalt, instead, is characterized by low Al/Ti ratios of <18 [*Engel et al.*, 1965]. We conclude that the detrital material within core LV28-42-4 is of continental origin.

[39] The molar Fe/Al ratios of core LV28-42-4 range around 0.28 (mol/mol) ±0.03 (Table 3), corresponding to average Fe/Al ratios of aerosols from various continental areas (~0.28 [*Pye*, 1987]), and being close to 0.2 from SE Asian (Nanking) loess deposits [*Taylor et al.*, 1983] and 0.21 of the North American shale composite [*Gromet et al.*, 1984]). The Fe/Al ratios of core LV28-42-4 are clearly lower than both the core top Fe/Al ratios of 0.35–0.44 from the deep central basin of the Sea of Okhotsk (Nürnberg, unpublished data, 2004), and average pelagic clay (~0.37 [*McLennan*, 1995]). Oceanic crust Fe/Al ratios, in contrast, are even lower (<0.15 [*Engel et al.*, 1965]). As the core LV28-42-4 Fe/Al values compare well with values reported for eolian dust and wind-transported deposits, we conclude that the Sea of Okhotsk sediments involve an eolian sediment component.

4.1.3. Fluxes

[40] The accumulation rates of siliciclastics and >63 μm fraction reflect temporal changes in the supply of terrigenous material to the central Sea of Okhotsk (Figure 7). Accumulation rates of siliciclastics range between ~2–16 g cm^{-2} kyr^{-1} at Site MD01-2415, while being consistently lower at the southern site LV28-42-4 (~1–6 g cm^{-2} kyr^{-1}). Core top values are 6 g cm^{-2} kyr^{-1} and 4.5 g cm^{-2} kyr^{-1}, respectively. Both cores have in common the relative increase in terrigenous matter accumulation during late glacial times, within the terminations (best seen during Termination I, II, IIIa, III and IV), and the subsequent early interglacial climatic optima (e.g., MIS 1.1, 5.5, 7.3, 9.3). During full glacial conditions, accumulation of

[1] Auxiliary data are available electronically at World Data Center-A for Paleoclimatology, NOAA/NGDC, 325 Broadway, Boulder, CO 80303, USA (paleo@mail.ngdc.noa.gov; URL: http://www.ngdc.noaa.gov/paleo).

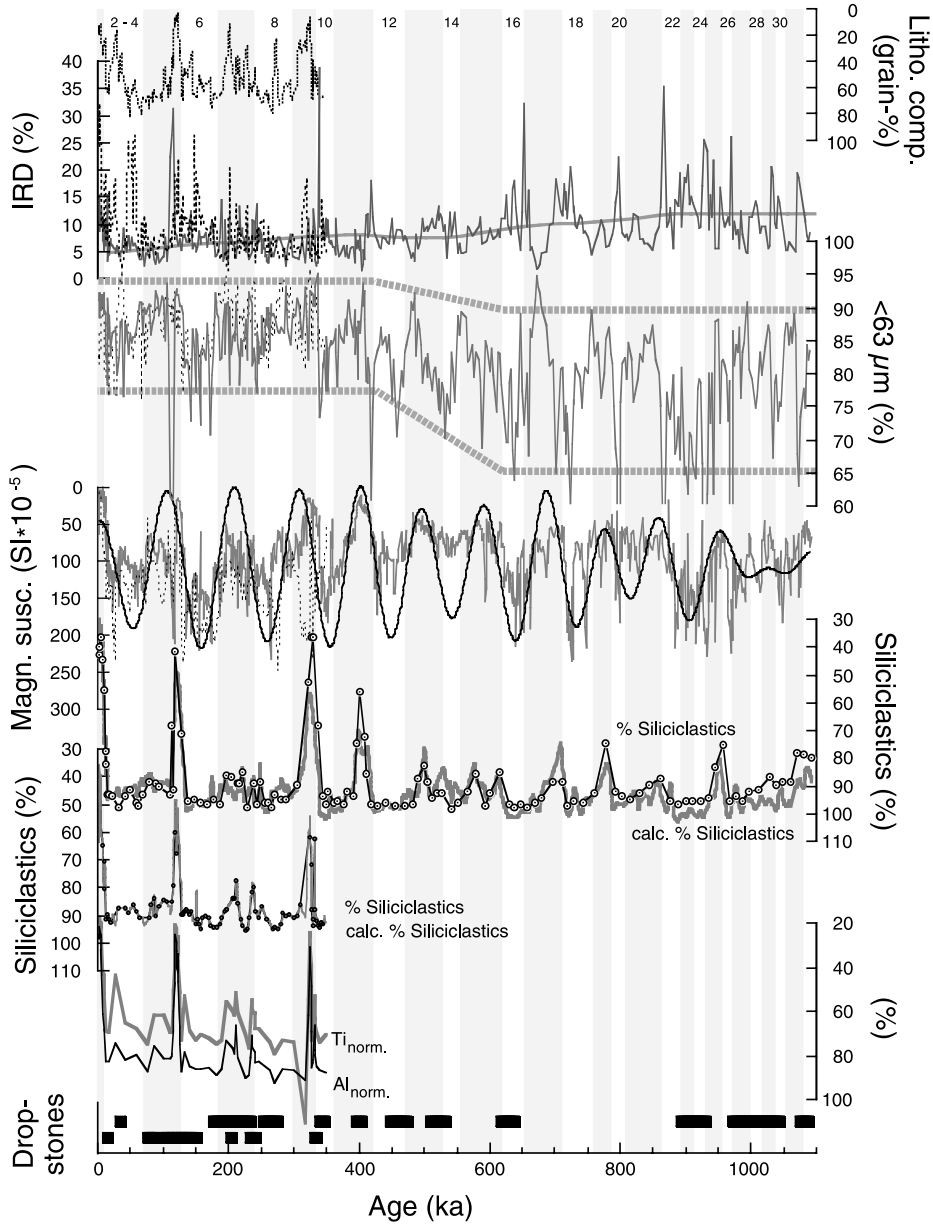

Figure 6. Temporal variations of terrigenous proxy data from cores LV28-42-4 (last ~350 kyr) and MD01-2415 (last ~1100 kyr). In both cores, titanium and aluminum concentrations (normalized to average Russian Paleozoic shale titanium and aluminum concentrations [*Ronov and Migdisov*, 1971]), magnetic susceptibility records, percentages of siliciclastics, and the grain percentages of lithogenic components [*Kaiser*, 2000] correlate, reflecting glacial/interglacial variations. Note scales are inversely plotted. The magnetic susceptibility is inversely correlated to the <63 μm fraction. The filtered 100 kyr component of magnetic susceptibility values of core MD01-2415 implies variations in response to the Earth's eccentricity fluctuations at least for the last ~500 kyr. In order to derive a better temporal resolution, percentages of siliciclastics were also calculated by using the high-resolution opal data set derived from shipboard color b* and mean sampled $CaCO_3$ and TOC records. Ice-rafted debris (IRD) is reflected by the 125–500 μm fraction (in percent of the siliciclastic fraction). Solid bars indicate the abundance of large, ice-rafted dropstones (−5 cm in diameter). Thick dashed lines point to a general fining in grain size after ~600–400 ka. The shaded line underlying the IRD record is the weighted smooth of the *Krissek* [1995] IRD record of North Pacific ODP Site 881. Shaded areas indicate interglacial periods. Numbers delineate marine oxygen isotope stages.

Table 3. Elemental Ratios for Core LV28-42-4

	Fe/Al	Al/Ti
Mean	0.28	35.9
Standard deviation	0.03	3.1
Maximum	0.33	45.0
Minimum	0.19	23.8

terrigenous matter was significantly reduced. Accumulation rates of the fine fraction (<63 μm) ranging between 1–20 g cm^{-2} kyr^{-1} exhibit a similar trend with commonly higher accumulation rates at core location MD01-2415. IRD accumulation (125–500 μm size fraction) corresponds to the temporal variations in lithogenic component accumulation rates (Figure 7), but appears to be lower at site LV28-42-4 than at site MD01-2415.

[41] At core location LV28-42-4, iron accumulation rates are in the range of 20–100 mg cm^{-2} kyr^{-1} over most of the time period studied. The core top value is 198 mg cm^{-2} kyr^{-1}, while averaged over the last 10 kyr it decreases to ~100 mg cm^{-2} kyr^{-1}. During terminations, maximum values of up to 280 mg cm^{-2} kyr^{-1} can be observed.

4.2. Temporal and Spatial Changes in Marine Productivity

[42] The assessment of past marine productivity in the study area results from the parallel measurement of various parameters approximating paleoproductivity, and the subsequent calculation of proxy accumulation rates. Because of the dominance of terrigenous flux over most of the time span covered by our cores, all productivity proxies show low concentrations except during deglaciations and interglacial/interstadial times of extremely enhanced paleoproductivity. Opal and $CaCO_3$ concentrations vary up to ~60% and ~20%, respectively (Figure 8). These concentrations are consistent with data of *Ternois et al.* [2001], *Gorbarenko et al.* [2002], and *Narita et al.* [2002], who studied the last glacial/interglacial cycle in the Sea of Okhotsk. The extremely high opal concentrations during the warm periods is caused by a high

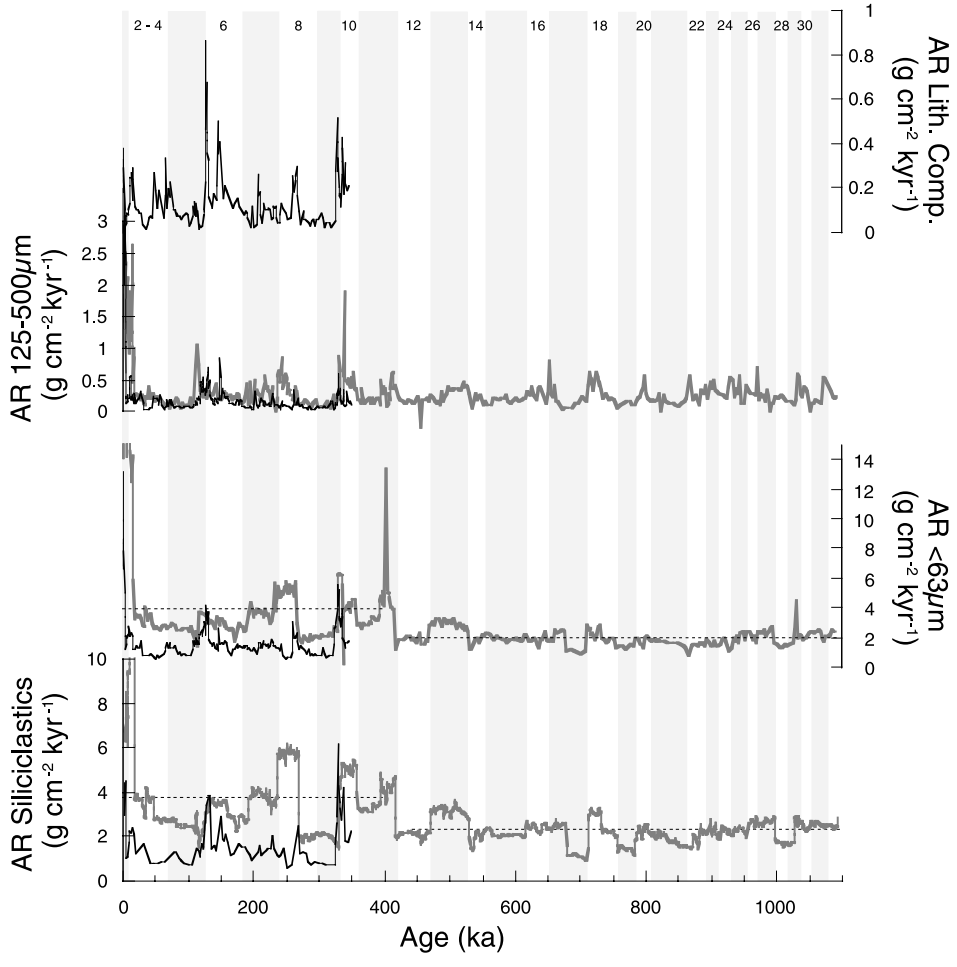

Figure 7. Mass accumulation rates of siliciclastics, the fine fraction (<63 μm), IRD (defined as the 125–500 μm fraction in percent of the siliciclastic fraction), and lithogenic components for cores LV28-42-4 and MD01-2415. Dashed lines indicate a change in average accumulation rates of siliciclastics and the fine fraction between 400 and 500 ka. Shaded areas indicate interglacial periods. Numbers delineate marine oxygen isotope stages.

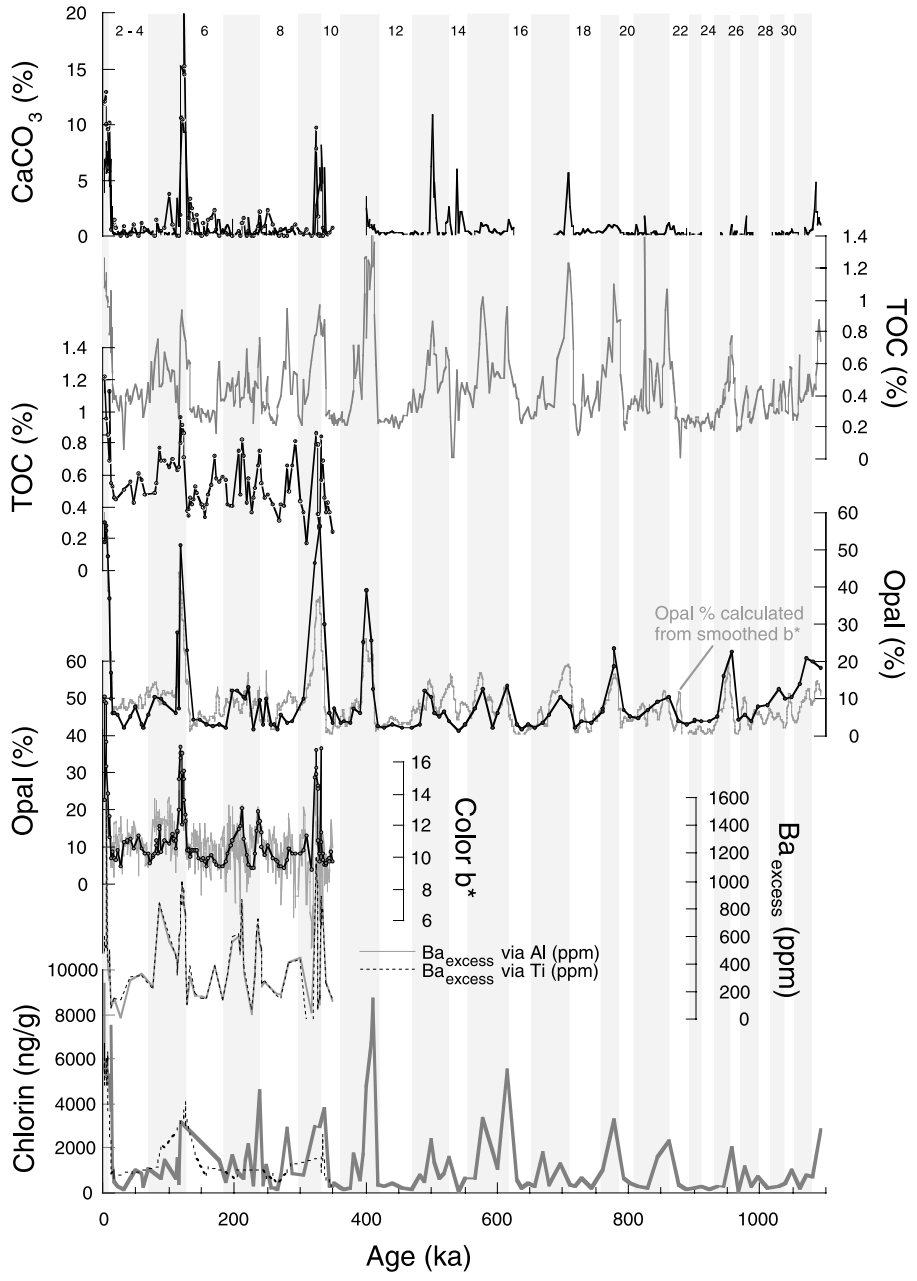

Figure 8. Temporal variations of chlorins, Ba_{excess}, opal, TOC, and $CaCO_3$ of cores LV28-42-4 (short data records) and MD01-2415. The opal record of LV28-42-4 is underlain by sediment color b* (shaded curve). The high-resolution opal data set for core MD01-2415 is converted from the sediment color b* values according to the equation opal (%) = −14.17 + 4.65 b*; where r = 0.94. Ba_{excess}, which is available only for core LV28-42-4, was calculated by correcting total barium (Ba_{tot}) for the nonbiogenic portion according to $Ba_{excess} = Ba_{tot} - (Al \times 0.0065)$ and $Ba_{excess} = Ba_{tot} - (Ti \times 0.126)$ [e.g., *Nürnberg et al.*, 1997a], where 0.0065 and 0.126 are the global mean Ba/Al and Ba/Ti ratios of alumosilicates, respectively [*Wedepohl*, 1991]. Shaded areas indicate interglacial periods. Numbers delineate marine oxygen isotope stages.

siliceous plankton (diatom, radiolaria) contribution [e.g., *Matul et al.*, 2002]. The presence of $CaCO_3$ is mainly related to planktonic (average 8 grain % [*Kaiser*, 2000] and benthic (average 4 grain %) [*Kaiser*, 2000]) foraminifer abundances. It appears that interglacial/interstadial $CaCO_3$ peaks at core LV28-42-4 commonly exceed the maximum concentrations at core MD01-2415. In turn, interglacial/interstadial opal concentrations are higher at location MD01-2415 compared to the more southern position of core LV28-42-4.

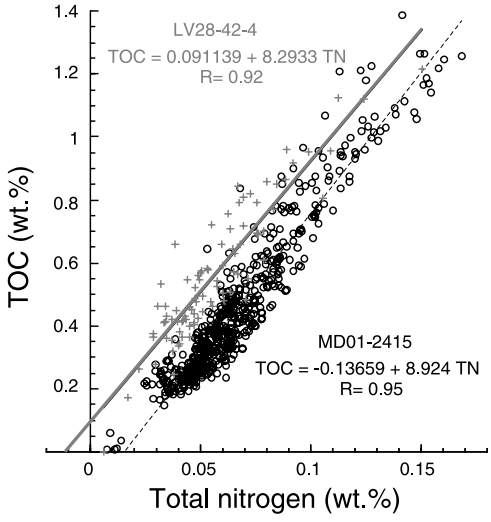

Figure 9. The %TN versus %TOC for cores MD01-2415 (circles) and LV28-42-4 (crosses). The %TN intercept at %TOC = 0 reflects the percent of inorganic nitrogen (IN) associated with the sediments. The intercept values were used to calculate the nitrogen content of the sedimentary organic matter (organic nitrogen %ON = %TN − %IN) according to *Goñi et al.* [1998].

[43] TOC exhibits maximum values of 1.4% during the warm periods, while concentrations are commonly below 0.6% during the remaining time. TOC concentrations are consistently higher in core LV28-42-4 than in core MD01-2415 at similar total nitrogen (TN) concentrations (Figure 9). In core MD01-2415, the atomic ratios between carbon and nitrogen ([C/N]a) are commonly between 5 and 9, and initially imply a marine source of sedimentary organic carbon through most of the time studied. Similar [C/N]a ratios were reported by *Ternois et al.* [2001] and *Seki et al.* [2003] for the last glacial/interglacial cycle in the southern Sea of Okhotsk. For core LV28-42-4, instead, the [C/N]a ratios are mainly >10 pointing to terrigenous sources for TOC. As the presence of clay-bound nitrogen components, including inorganic ammonium [*Müller*, 1977], may affect the [C/N]a ratios, we corrected the TN concentrations for inorganic nitrogen.

[44] For both cores, the relationships between %TN *versus* %TOC are linear (r = 0.92 for LV28-42-4; r = 0.95 for MD01-2415; Figure 9). For core MD01-2415, the positive %TN intercept of 0.015 at zero %TOC implies that a distinct fraction of the nitrogen present in the sediments is inorganic. In order to correct for this inorganic (terrigenous) nitrogen source, we subtracted the quantity of inorganic nitrogen inferred from the %TN intercept from the measured %TN values (according to *Goñi et al.* [1998]). In consequence, the corrected [C/N]a ratios for MD01-2415 sediments increase and become more equivocal as indicators of marine organic matter (Figure 10). For core LV28-42-4 sediments, instead, [C/N]a ratios were not corrected for inorganic nitrogen, as we observe a negative %TN intercept of 0.01 at zero %TOC. After the correction for inorganic nitrogen, [C/N]a ratios of both cores converge to values between ~10 and 15 (maximum 20) suggesting that the central Sea of Okhotsk sediments contain considerable amounts of terrestrial organic matter (Figure 10). This is in agreement to biomarker studies of *Ternois et al.* [2001], who suggest that sediments from the last deglaciation are relatively more associated with terrestrial organic material.

[45] Chlorin concentrations show maximum values of >10,000 ng/g during the Holocene, while during older interglacials/interstadials chlorin concentrations (<9000 ng/g) never reach the Holocene concentrations (Figure 8). Full glacial periods exhibit chlorin concentrations of below 1000 ng/g. The good match between chlorin and TOC concentrations (Figure 9), however, implies that chlorins may include a considerable terrestrial component.

[46] Biogenic barium (Ba_{excess}) is ranging between 0–1600 ppm with 200–400 ppm during the cold periods and maximum values during interglacial/interstadial periods (Figure 8). During peak interglacial times, Ba_{excess} concentrations amount to 1000–1600 ppm, which by far exceeds Ba_{excess} concentrations found in other high-productivity areas like the Antarctic Zone and Polar Frontal Zone in the Southern Ocean (max. 800–1000 ppm) [*Nürnberg et al.*, 1997a]. The downcore variability in Ba_{excess} matches the TOC record (r > 0.74). The correlation to opal is r = 0.78.

[47] Glacial/interglacial variations in export production were finally interpreted from the calculation of accumulation rates of the various proxy data (Figure 11). We observe significant productivity events during glacial terminations I, II, III, IIIa, IV, and V, and the subsequent interglacial climatic optima MIS 1.1, 5.5, 7.3, 7.5, 9.3, 11.3. Further back in time, productivity maxima are less pronounced, but are still recognizable during MIS 13, 15, 17, 19, 21, 25 and 31. Most of these productivity maxima are well reflected in accumulation rates of all productivity proxies measured (chlorin, Ba_{excess}, opal, TOC, and $CaCO_3$), and are higher by a factor of 5–10 compared to full glacial values. The $CaCO_3$ data appear to be least reliable for export productivity reconstructions most presumably due to carbonate dissolution. In particular during MIS 7.3 and MIS 7.5, $CaCO_3$ peaks are lacking although other productivity proxies point to enhanced export production.

[48] Mass accumulation rates of TOC and $CaCO_3$ range between 0–0.2 g cm^{-2} kyr^{-1} and 0–1.5 g cm^{-2} kyr^{-1}, respectively. The Holocene TOC values of >0.2 g cm^{-2} kyr^{-1} and $CaCO_3$ values of >0.5 g cm^{-2} kyr^{-1} compare to data of *Gorbarenko* [1996] and *Gorbarenko et al.* [2002] from more southern site locations. Opal and Ba_{excess} accumulation rates range between 0–6 g cm^{-2} kyr^{-1} and 0–0.008 g cm^{-2} kyr^{-1}, respectively, with maxima during warm periods. Accumulation rates of chlorin are between $0–10 \times 10^{-5}$ g cm^{-2} kyr^{-1}. Productivity peaks best reflected in chlorin, opal, and carbonate accumulation rates appear to be more pronounced during the last ~500 ka.

[49] As the TOC concentrations are considerably contaminated by terrestrial organic carbon, the calculation of marine paleoproductivity from TOC is erroneous. Hence we calculated export production (P_{new}) from Ba_{excess} concentrations. P_{new} is commonly <10 gC m^{-2} yr^{-1} during the cool periods, and increases to >20 gC m^{-2} yr^{-1} during

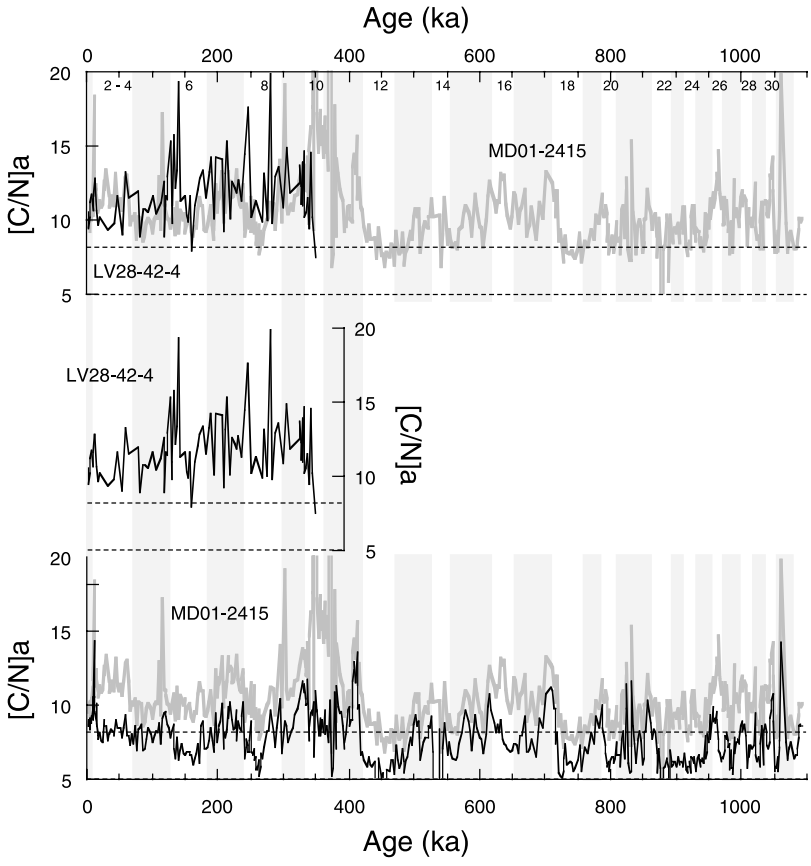

Figure 10. Initial [C/N]a ratios (thin lines) for cores MD01-2415 (long record, bottom diagram) and LV28-42-4 (short record, middle diagram). Thick line in bottom diagram indicates [C/N]a ratios of core MD01-2415 corrected for clay-bound inorganic nitrogen. Stippled lines depict [C/N]a ratios of 5–8 typical for marine organic matter. The top diagram shows the converged [C/N]a records of both cores corrected for inorganic nitrogen. The high [C/N]a ratios imply a considerable contribution of terrestrial organic carbon to the central Sea of Okhotsk sediments.

deglaciations and succeeding climatic optima. Maximum values of ~110–140 gC m^{-2} yr^{-1} appear during MIS 9 and the Holocene, respectively, although these values may be overestimated due to reasons discussed above. In general, the calculated interglacial P_{new} is comparable to modern values of annual export production in the Sea of Okhotsk (see http://jpac.whoi.edu/images/honjo.pdf) and to reconstructions for the seasonally ice-covered areas in the Southern Ocean [*Gingele et al.*, 1999].

4.3. Synthesis: Environmental Change in the Sea of Okhotsk Over the Last 1.1 Myr

[50] Our studies reveal the glacial/interglacial environmental changes in the Sea of Okhotsk over the last ~1.1 Myr. These changes are expressed by a coupled interplay between atmospheric circulation patterns, sea ice dynamics, terrigenous flux, and surface productivity.

[51] The seasonally sea ice–covered Sea of Okhotsk depositional environment is mainly characterized by the predominant flux of terrigenous material (up to 90%) during the past 1.1 Myr. Various terrigenous sources and transport processes can be identified, whereupon ice rafting appears as the most apparent transport agent for terrigenous material, primarily indicated by the continuous presence of large dropstones in our cores (Figure 6). Erosional processes like fluvial discharge, wind transport, surface and bottom currents, and reworking and resuspension processes along the shelf break in response to sea level changes further contribute to the hemipelagic sedimentation, but have different significance for the central Sea of Okhotsk.

[52] From a suite of downcore records covering large parts of the Sea of Okhotsk, *Kaiser* [2000] and *Gorbarenko et al.* [2002, 2003] already deduced that coarse ice-rafted material is distributed basin-wide. From the observation that most large (3–5 cm) dropstones found in the Sea of Okhotsk sediments appear well rounded, we deduce that they most likely originate from beach deposits. Thus bottom adfreezing, anchor ice, and beach ice formation [e.g., *Pfirman et al.*, 1990] may be considered as the dominating entrainment mechanisms for these pebbles. The wide, tidal-dominated (6 m tidal range [*Kowalik and Polyakov*, 1998]) northern shelf areas allow for the effective and large-scale entrainment of lithogenic shelf material into sea ice, which is subsequently transported offshore according to the cyclonal surface current system, strong tidal currents, and the predominant atmospheric circulation pattern. During summer the

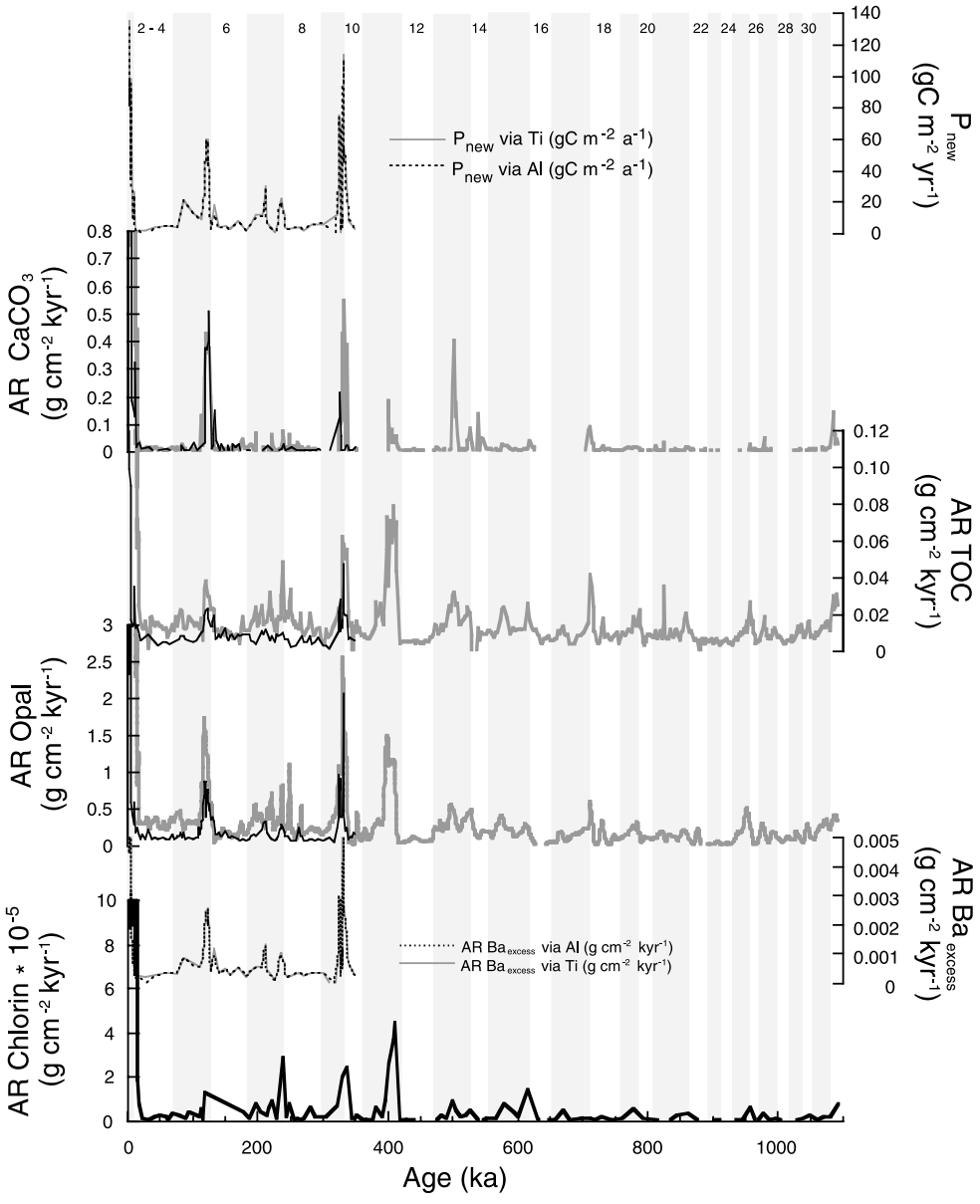

Figure 11. Accumulation rates of chlorin, Ba_{excess}, opal, TOC, and $CaCO_3$ in comparison to bulk accumulation rates for cores LV28-42-4 (short data records) and MD01-2415. Export production (P_{new}) was assessed from Ba_{excess} using the equation of *Nürnberg* [1995]: $P_{new} = 3.56 ((AR_{Baexcess}/0.209 \log (AR_{bulk})) - 0.213))^{1.504} z^{-0.0937}$, where AR is the accumulation rate ($\mu g\ cm^{-2}\ yr^{-1}$) and z is water depth (m).

lithogenic freight is released from sea ice, and contributes to the siliciclastic fraction of the deep-sea sediments.

[53] Whether icebergs contributed to the flux of IRD through time is not well studied. We may, however, largely exclude iceberg transport for the modern/Holocene and last glacial environment. Today, only mountain glaciers ($\sim$1500 km^2, >1500 m NN) are present on Kamchatka Peninsula and across the East Siberian hinterland (World Glacier Inventory, National Snow and Ice Data Center, University of Colorado) and even during the last glacial maximum, these mountain glaciers never reached sea level [*Frenzel et al.*, 1992]. During MIS 4, *Braitseva and Melekestsev* [1974] describe coastal glaciers along the eastern coast of Kamchatka, which affected the IRD flux in the North Pacific [*St. John and Krissek*, 1999], but not in the Sea of Okhotsk.

[54] Iceberg transport might have been more important during older glacials, when the northern and eastern coastal regions of the Sea of Okhotsk as well as Kamchatka were glaciated [*Braitseva and Melekestsev*, 1974; *Ananjev et al.*, 1984]. During mid-Pleistocene times, mountain glaciers of predominantly alpine character most probably reached down to sea level along western Kamchatka as testified by extended moraine deposits [*Zech et al.*, 1996, 1997], and

might have served as prominent source areas for ice-rafted debris. In particular during MIS 6, the IRD accumulation in core LV28-42-4 is 2–3 times higher than in other glacials (Figure 7) and points to considerable changes in the IRD transport processes [*Nürnberg et al.*, 2003]. These observations are in agreement with the southward progression of the Polarfront in the NW Pacific during "superglacial" MIS 6 [*Kent et al.*, 1971; *Thompson and Shackleton*, 1980; *Thompson*, 1981].

[55] Besides ice rafting, eolian transport appears as an important mechanism to contribute siliciclastic material to the Sea of Okhotsk environment. From the comparison of average Holocene iron accumulation rates of ~100 mg cm^{-2} kyr^{-1} (this study) and the modern atmospheric iron fluxes in the Sea of Okhotsk of ~24 mg cm^{-2} kyr^{-1} roughly estimated from *Gao et al.* [2001] (alternatively, ~10–100 mg cm^{-2} kyr^{-1} proposed by *Duce and Tindale* [1991]), we conclude that eolian dust may contribute significantly to sedimentation.

[56] In fact, the modern eolian flux to the remote, ice-free NW Pacific (north of 43°N, 150–164°E) is assessed from sediment traps to ~0.9–1.8 g m^{-2} yr^{-1} (annual lithogenic flux [*Saito et al.*, 1992]), and from marine records to 2.1 g m^{-2} yr^{-1} [*Leinen*, 1989]) (both in compilation of *Mahowald et al.* [1999]). These values are considered to be minimum values, and eolian flux in the Sea of Okhotsk is presumably higher as being closer to potential source areas of wind-transported dust. *Duce et al.* [1991] assess the eolian dust flux to ~10 g m^{-2} yr^{-1} in the Sea of Okhotsk. By now, we are not able to quantify the eolian contribution in our cores, but it for sure needs to be considered, specifically in terms of glacially strengthened wind activity. *Hovan et al.* [1991] suggested a fivefold increase in dust input to the NW Pacific during glacials. Simulations of *Mahowald et al.* [1999] show a 2.5-fold higher dust loading and, specifically for high latitudes, a twentyfold higher loading, during the last glacial maximum relative to present. The high dust deposition during glacial times is best explained by the tight interplay between the increasing extent of unvegetated areas serving as source areas, the more vigorous atmospheric circulation with increasing entrainment and transport efficiency, and finally, the weakened hydrological cycle with lowered precipitation rates [*Mahowald et al.*, 1999].

[57] The large Amur River system entering the northwestern part of the Sea of Okhotsk is today characterized by a high sediment loading [*Holeman*, 1968; *Milliman and Meade*, 1983; *Anikiev et al.*, 2001], and effectively influences the sea surface hydrography (Russian Federal Research Institute of Fisheries and Oceanography, 2001), marine productivity (NASA, SeaWIFS Project, 1998), sea ice distribution [*Ogi et al.*, 2001] and sedimentation rates along northern Sakhalin [*Kaiser*, 2000; *Kozdon*, 2002]. Several indications, however, suggest that the central Sea of Okhotsk coring locations were not affected by fluvial sediment supply. In fact, the extremely high sedimentation rates of >60 cm kyr^{-1} seen over the past 8000 years along the shallow northeastern Sakhalin slope [*Kozdon*, 2002] suggest that the main path of fine river suspension is bent around the northern tip of Sakhalin and follows the southward flowing East Sakhalin Current. A surface near eastward transport of fluvial material toward the central parts of the Sea of Okhotsk is generally against the westward directed branch of the cyclonic surface water circulation and hence rather unlikely. Also, the potential transfer of fluvial sediments following the Sakhalin slope topography to the east is considered to result in accumulation within the deep Derugin Basin (1500 m water depth). A significant eastward transport from the Amur discharge area across Derugin Basin to our coring sites (>500 km distance), which are located at distinctly shallower water depths of ~800–1000 m, is not expected although it cannot be ruled out entirely. Generally, during full glacial and deglacial times, riverine input of terrestrial matter is considered to be reduced as precipitation was low and the Amur river was frozen over most of the time. Indeed, sedimentation rates on the western Sakhalin shallow slope were drastically reduced during the last glacial [*Kaiser*, 2000; *Kozdon*, 2002].

[58] The maximum accumulation rates of terrigenous material are bound to late glacials, deglaciations, and the subsequent early climatic optima (Figure 12), mainly in response to the continuously rising sea level during glacial/interglacial transitions. Previously deposited sediment on the gradually submerging shelf areas was reworked and resuspended, moved offshore via downslope tidal currents, surface and/or intermediate waters, and contributed to the hemipelagic sedimentation. The contribution of upper continental slope and shelf sediment to hemipelagic sedimentation is best testified by the terrestrial organic matter compound in central parts of the Sea of Okhotsk (Figure 10), but was supposedly less effective during full glacial times of lowered sea level. The deglacial maxima in terrigenous flux appear to be succeeded by or synchronous to high-productivity events, which is best expressed at terminations I, II, III, IIIa, IV and V. In a high-resolution biomarker study, *Ternois et al.* [2001] also showed the synchronous increase in terrigenous flux and marine productivity during Termination I, consistent with our results.

[59] Important to note is a descent in grain size after ~400–600 ka indicated by a gradual decline of the IRD fraction and an increase of the <63 μm fraction (Figure 6). This subtle change, which implies a change in the relative importance of the different transport mechanisms for siliciclastic material in the Sea of Okhotsk, compares to a gradual decrease in IRD concentrations in the North Pacific [*Krissek*, 1995] (Figure 6) and to a coarsening of loess grain sizes in SE Asia (Figure 13).

4.3.1. Glacial Scenario

[60] Our combined approach to reconstruct marine productivity and terrigenous flux allows us to define glacial, deglacial, and interglacial scenarios for the Sea of Okhotsk environment over the past 1.1 Myr. During glacials, sedimentation rates were commonly low, while the accumulation of terrigenous matter dominated. The strengthened atmospheric circulation [*COHMAP Members*, 1988], increased winter monsoon [*Wang et al.*, 1999], and a reduced summer insolation [*Berger and Loutre*, 1991] promoted sea ice formation. Analogous to the modern winter situation, we assume that during full glacial times a strong Siberian High and a pronounced Aleutian Low persisted. Such pairing of atmospheric pressure cells [*Godbole and Shukla*, 1981]

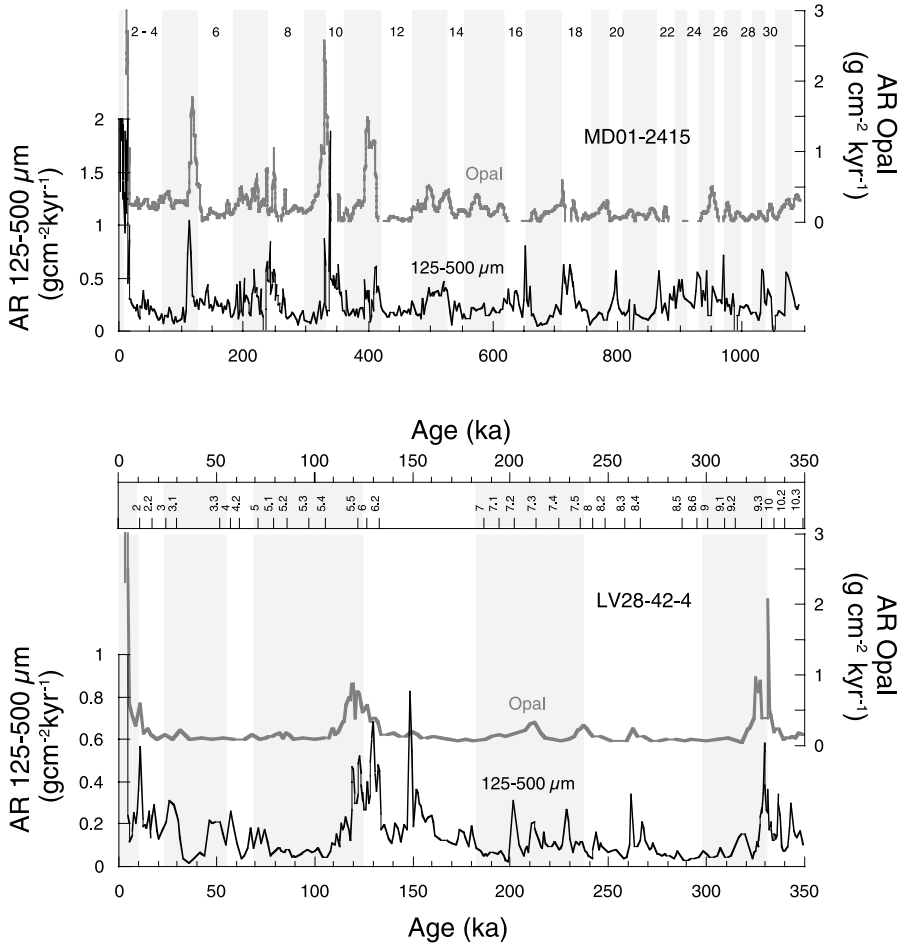

Figure 12. Comparison between temporal variations of terrigenous flux (here IRD accumulation rates indicated by the 125–500 μm fraction in percent of the siliciclastic fraction; thin curves) and opal accumulation rates approximating marine productivity (thick curves) of cores LV28-42-4 (bottom diagram) and MD01-2415 (top diagram). High-productivity events are predominantly preceded by or synchronous to high IRD fluxes and are best established during late glacial times, terminations, and/or succeeding early climatic optima. Shaded areas indicate interglacial stages (odd numbers).

caused predominant northerly wind directions in the Sea of Okhotsk area, which favored the formation of coastal polynias, and accelerated sea ice formation. In addition, the sea level–induced cessation of warm water mass transfer from the Sea of Japan through Soya Strait into the Sea of Okhotsk further amplified sea ice formation during glacial times. Areas of sediment entrainment into sea ice moved basinward as the shelves fell dry during glacial times of sea level lowstands. The Amur River runoff is suspected to be drastically reduced during these cold and dry climate conditions [*Hovan et al.*, 1991; *Ananjev et al.*, 1993] analogous to the today's winter situation, during which the river is frozen and runoff is only 1% of the summer runoff [*Ogi et al.*, 2001]. Such reduction in Amur freshwater discharge might have effectively controlled sea ice formation. For the modern environment, *Ogi et al.* [2001] observed that the inflow of warm Amur water during summer tends to raise the regional sea surface temperatures, causing less sea ice formation during the following winter period.

[61] The Siberian High pressure cell appears to effectively influence ice formation, wind intensity, precipitation, and hence terrigenous flux to the Sea of Okhotsk during glacial times. Today, the Siberian High is an extremely shallow, semipermanent, quasi-stationary atmospheric action center over northern Mongolia, which affects the Asian climate system during winter. Being primarily thermally induced in response to strong and continuous radiative cooling of the snow-covered Earth surface (F. Panagiotopoulos, The Siberian High: Variability, trends and teleconnections, available at http://www.nccr-climate.unibe.ch/download/events/suscho02/students_abstracts/Panagiotopoulos%20Fotis.htm), the Siberian High causes both the low-altitude dust storms that are primarily responsible for dust transport to the Chinese loess plateau (southeasterly directed SE Asian winter monsoon), and the high-altitude spring dust storms (east Asian jet stream) that transport dust for long distances over the North Pacific Ocean [*Rea*, 1994; *Reynolds and King*, 1995]. Indeed, *Ding et al.* [1995] related the loess-soil alterations in China to varying strengths of the SE Asian

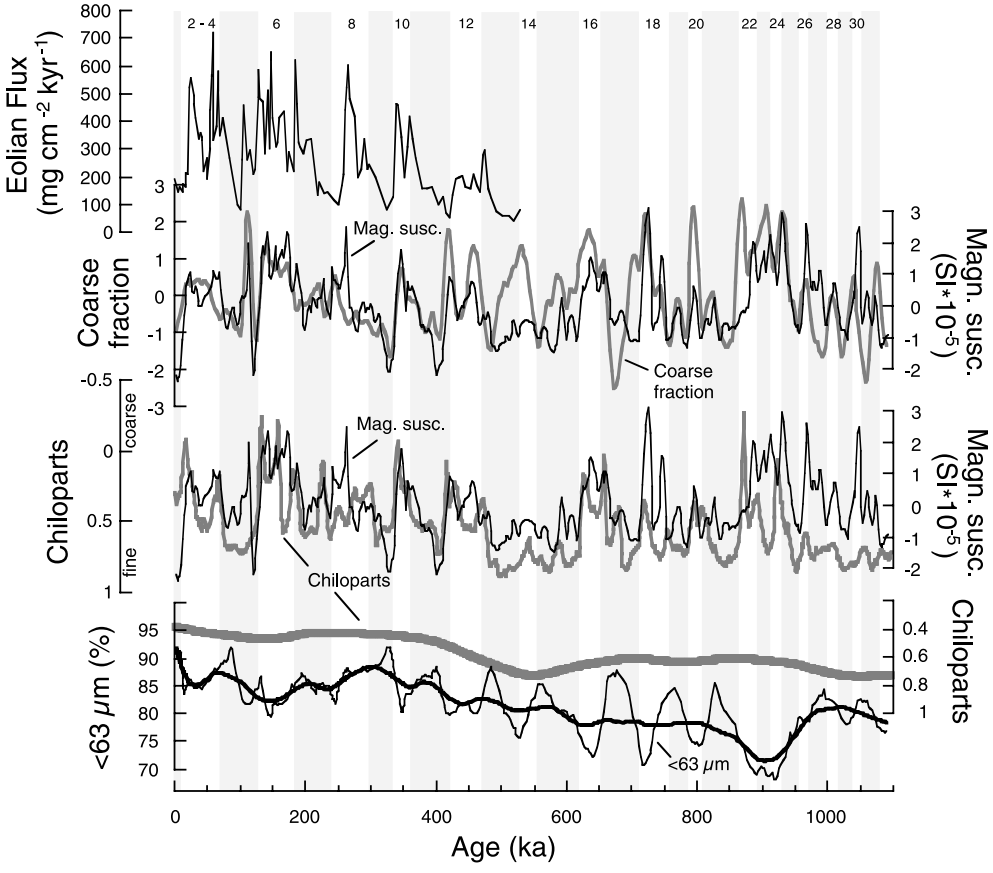

Figure 13. Comparison of the magnetic susceptibility and coarse fraction (>63 μm fraction in percent of the bulk sediment) records of core MD01-2415 (four-point smoothed, normalized to unit variance, removed linear trend), both reflecting terrigenous flux to the Sea of Okhotsk. The magnetic susceptibility record shows a good correlation to the normalized CHILOPARTS grain size record (thick, shaded lines) from China [*Ding et al.*, 2002]. Finer grain sizes correspond to higher values in the CHILOPARTS record. The Sea of Okhotsk records further match the eolian flux record of *Hovan et al.* [1991] from the northwest Pacific Ocean (core V21-146). The nine-point smoothed fine fraction record (<63 μm fraction in percent of the bulk sediment) exhibits a fining trend, which corresponds to a coarsening trend in the CHILOPARTS record during the last ~500 kyr (thick lines in bottom diagram represent weighted curve fits, smoothing factor 10%). Shaded areas indicate interglacial periods. Numbers delineate marine oxygen isotope stages.

winter monsoon. During glacial periods, expanded continental ice sheets and extended sea ice coverage in the Northern Hemisphere strengthened the Siberian High due to a downstream cooling effect [*Ding et al.*, 2002], and favored colder, drier, and stronger winter monsoon winds resulting in dry land expansion and higher depositional rates of coarse material. High-altitude and long-distance dust transport to the North Pacific via the SE Asian jet stream is apparently reflected in core V21-146 located ~2000 km to the south-southeast of the Sea of Okhotsk on Shatsky Rise [*Hovan et al.*, 1991]. Here dust flux maxima are of glacial age and directly downwind from China, whereas minima belong to interglacial periods. From North Pacific neodymium isotope studies and the direct link of times of enhanced dust flux at site location V21-146 to times of loess formation in China, *Jones et al.* [1994] and *Rea* [1994] deduced that the semiarid and arid regions of east central Asia are most likely the predominant sources of dust to the Pacific Ocean.

[62] The importance of the Siberian High as a pacemaker for both the terrigenous flux to the Sea of Okhotsk, and the alternating loess soil deposition in China is underlined by the convincing match between the magnetic susceptibility and fine fraction (<63 μm) records of core MD01-2415 and the CHILOPARTS (China loess particle timescale) grain size record from the China loess deposits [*Ding et al.*, 2002] (Figure 13). Each of the glacial/interglacial climatic cycles show a close match between the records, with only few exceptions. Both CHILOPARTS and the MD01-2415 records reveal precessional forcing. We therefore conclude that environmental change in both the Sea of Okhotsk area and China were closely coupled over the past 1.1 Myr via atmospheric teleconnections.

[63] Intensification and prolongation of sea ice formation processes during glacial times presumably affected the chemical and physical signature of water masses, and hence promoted sea surface cooling, brine rejection and intermediate water formation [*Wong et al.*, 1998]. Today, SOIW exits through the Kurile passages and serves as a significant source for the salinity minimum and oxygen maximum present in the NW Pacific Intermediate Water [*Talley*, 1991]. *Keigwin* [1998] found indications from benthic foraminiferal $\delta^{18}O$ and $\delta^{13}C$ for a better ventilated water mass at intermediate depths in the glacial northwestern Pacific. In accordance to that, the presence of the radiolarian genus *Cycladophora davisiana* in glacial Sea of Okhotsk sediments, which today is limited to the upper part of the SOIW between 200–500 m [*Nimmergut and Abelmann*, 2002], suggest that intermediate water formation persisted during glacial periods. Benthic foraminiferal $\delta^{13}C$ [*Keigwin*, 1998] and Cd/Ca data [*Boyle*, 1988] imply better ventilated and nutrient-depleted intermediate waters in the Sea of Okhotsk for the last glacial maximum.

[64] From the continuous presence of IRD in the sediment cores studied, we infer a seasonally varying and mobile sea ice cover even during full glacial times. For glacial MIS 2, *Shiga and Koizumi* [2000] concluded from diatom studies that the eastern part of the Sea of Ohkotsk was ice-free. The sea ice cover might have been annual and rigid in some northernmost parts of the Sea of Okhotsk [*Kaiser*, 2000].

[65] Both, the extended sea ice and the reduced Amur River discharge confined nutrient supply to the central parts of the Sea of Okhotsk. In addition, light limitation related to the extended (snow covered) sea ice, and the strengthened vertical water column mixing reduced nutrient utilization by planktonic organisms. Export productivity calculated from Ba_{excess} during full glacial stages was >5 gC m^{-2} yr^{-1}.

4.3.2. Deglacial Scenario

[66] During glacial terminations, we observe significant environmental changes in both cores studied (best seen at MIS12/11, MIS10/9, MIS 6/5 and MIS2/1 transitions). The flux of ice-rafted detritus increased significantly, accompanied by or slightly temporally lagged by increasing opal accumulation rates (Figure 13). The climatic amelioration led to a dynamic and mobile sea ice cover with northward propagating oscillating ice margins. Entire loads of ice-rafted detritus contributed to the deep-sea sedimentation during summer thawing and even during winter at the marginal ice zone. Synchronously, river runoff gradually incremented after full glacial conditions. Both, sea ice thawing and fluvial runoff caused surface freshening and the stabilization of the water column. Enhanced precipitation as indicated by pollen studies [*Heusser and Morley*, 1985] further contributed to lowered surface salinities and terminated convective mixing. High numbers of the radiolaria *C. davisiana* (70%) during the last deglaciation (Abelmann, unpublished data, 2001) point to water column stratification and to the formation of a dichothermal layer. Today, the dichothermal layer is at 20–200 m during summer, characterized by a temperature minimum as a relic of the winter convection, and embedded between extremely warm surface waters (16°–17°C), and 2°–3°C warmer water masses below.

[67] Nutrient concentrations in surface waters were presumably high during deglacial time periods, provided by fluvial discharge, ice rafting, and enhanced terrigenous flux from the successively flooded shelves. According to *Appollonio* [1973] and *Jacobs et al.* [1979], sea ice may provide nutrients such as nitrate, ammonia and silicate at concentrations an order of magnitude higher than in ambient seawater. Both, the high nutrient concentration and the stable surface water stratification were prerequisites for an effective nutrient utilization, and hence promoted phytoplankton growth. Marine export production increased to >20 gC m^{-2} yr^{-1}.

[68] Our observations are in accordance to early studies of *Gorbarenko et al.* [1988], who described deglacial productivity spikes in the Sea of Okhotsk. Evidence for higher productivity in the NW Pacific on glacial/interglacial transitions was also reported by *Pisias and Leinen* [1984], *Tiedemann and Haug* [1995], and by *Keigwin* [1998]. The temporal changes in productivity in the Sea of Okhotsk closely follow variations in Earth's orbital precession, with productivity maxima generally occurring during precessional minima (maxima in Northern Hemisphere summer insolation). During the past ~400–500 ka productivity maxima became clearly pronounced at the end of glacial terminations, matching the amplified late Pleistocene 100 kyr variability in global ice volume.

4.3.3. Interglacial Scenario

[69] After the deglacial productivity events coupled to maxima in terrigenous flux, marine productivity continuously decreased to lower values, although they commonly remain higher than during full glacial periods. This observation is consistent with the last deglaciation study of *Ternois et al.* [2001], who observed an increase in marine biomarker accumulation rates during the deglaciation, and their subsequent decrease. Apparently, environmental conditions leading to extreme productivity events as observed during deglaciations, never returned. Nevertheless, interglacial periods are characterized by an enhanced marine productivity and a lowered IRD flux, induced by strengthened river discharge, and a seasonal and mobile sea ice cover comparable to the today's situation. For full interglacial periods, we assume that the inflow of warm and saline waters from the Japan Sea to the Sea of Okhotsk intensified convective mixing in the water column and caused nutrient replenishment and subsequent phytoplankton growth [*Ternois et al.*, 2001]. Analogous to the modern summer atmospheric circulation pattern of a pronounced Mongolian Heat Low and a strong Hawaiian High, we assume a prevailing SE monsoon and a considerable northward shift of the Intertropical Convergence Zone [*Wakatsuchi and Martin*, 1990] during interglacial times. In consequence, precipitation rates should have increased in the Amur drainage area leading to an enhanced freshwater discharge to the Sea of Okhotsk.

5. Conclusions

[70] During the past 1.1 Myr, the glacial/interglacial environmental changes in the Sea of Okhotsk are charac-

terized by a coupled interplay between atmospheric circulation patterns, sea ice dynamics, terrigenous flux, and surface productivity. The establishment of robust stratigraphies based on AMS ^{14}C dating, benthic $\delta^{18}O$ stratigraphy, and orbital tuning was an essential prerequisite to quantify the terrigenous flux and to assess paleoproductivity.

[71] Sedimentation in the Sea of Okhotsk is dominated by terrigenous material of continental origin. Both cores studied reveal similar patterns of temporal variability in terrigenous flux. Various terrigenous sources and transport processes were identified. Ice rafting appears as the most apparent transport agent for terrigenous material, primarily indicated by the continuous presence of large dropstones in the cores. The ice-rafted debris, which contributes significantly to the normal hemipelagic sedimentation, most likely originates from beach deposits. Coastal adfreezing along the wide, tidal-dominated northern shelf areas is considered as an effective and large-scale entrainment mechanism of lithogenic shelf material into sea ice. The debris is subsequently transported offshore according to the cyclonal surface current system, strong tidal currents, and the predominant atmospheric circulation pattern. During summer, the lithogenic freight is released from sea ice, and adds to the siliciclastic fraction in the deep-sea sediments. From the continuous presence of IRD in the sediment cores studied, we infer a seasonally varying and mobile sea ice cover even during full glacial times. Beside ice rafting, eolian transport appears as a further viable mechanism to contribute terrigenous material to the hemipelagic sedimentation in the Sea of Okhotsk.

[72] The monotonous siliciclastic-dominated sequences are interrupted by short, interglacial/interstadial events of extremely enhanced marine productivity, which correspond to precessional minima, and became increasingly pronounced during the past ~400–500 ka. The highest accumulation rates of terrigenous matter commonly occur during deglaciations and the subsequent early climatic optima. The periods of high terrigenous flux appear to be succeeded by or synchronous to the high-productivity events.

[73] Significant productivity events as reflected in accumulation rates of chlorin, Ba_{excess}, opal, TOC, and $CaCO_3$, occur during glacial terminations I, II, III, IIIa, IV, and V, and the subsequent interglacial climatic optima MIS 1.1, 5.5, 7.3, 7.5, 9.3, 11.3. During these events, accumulation rates of productivity proxies are higher by a factor of 5–10 compared to full glacial values. Further back in time, productivity maxima are less pronounced, but are still recognizable during the climatic optima. At ~400–600 ka, a subtle change in grain size and IRD contribution is observed, pointing to a change in transport mechanisms for the terrigenous material.

[74] Analogous to the modern winter situation, we speculate that during full glacial times a strong Siberian High and a pronounced Aleutian Low persisted. Such constellation of atmospheric pressure cells caused the strengthening of the atmospheric circulation. Predominant northerly wind directions, reduced Amur River discharge, and a lowered summer insolation favored the formation of coastal polynias, and accelerated sea ice formation. Our hypothesis is based on the match between our record of terrigenous flux to the Sea of Okhotsk (core MD01-2415) and the grain size record from the China loess deposits (CHILOPARTS), which is essentially a reflection of winter monsoon intensity. Environmental change in both the Sea of Okhotsk area and SE Asia were closely coupled over the past 1.1 Myr via atmospheric teleconnections, and our long sediment record appears to reflect the seesaw between Siberian High and Aleutian Low through time.

[75] Distinct changes in the depositional environment occurred during glacial/interglacial transitions. The flux of terrigenous matter increased significantly, accompanied by or slightly temporally lagged by increasing marine productivity. The climatic amelioration led to a dynamic and mobile sea ice cover with northward propagating oscillating ice margins. Sea ice thawing and fluvial runoff promoted the terrigenous flux and nutrient supply, caused surface freshening, and the stabilization of the water column. Both, the high nutrient concentrations and the stable water column stratification were prerequisites for an effective nutrient utilization and hence promoted phytoplankton growth.

[76] Interglacial periods are characterized by an enhanced marine productivity (although being considerably lower than during the terminations), and a lowered IRD flux, induced by strengthened river discharge, and a seasonal and mobile sea ice cover comparable to the modern situation. The inflow of warm and saline waters from the Japan Sea to the Sea of Okhotsk contributed to convective mixing in the surface waters, and caused nutrient replenishment and subsequent phytoplankton growth. Analogous to the modern summer atmospheric circulation pattern of a pronounced Mongolian Heat Low and a strong Hawaiian High, we assume prevailing SE monsoonal winds and a considerable northward shift of the Intertropical Convergence Zone during interglacial times. Hence precipitation rates should have increased in the Amur drainage area leading to an enhanced freshwater discharge to the Sea of Okhotsk.

[77] **Acknowledgments.** Funding of this research was provided by the German Science Foundation (DFG) within the authors' project Ti240/11-1 and by the Ministry of Science and Technology (BMBF) within the authors' projects KOMEX I and II. We thank Yvon Balut, Agnes Baltzer, and the Shipboard Scientific Party of RV *Marion Dufrèsne* cruise WEPAMA 2001 for their kind support. Also, we thank the Russian crew and Shipboard Scientific Party of RV Akademik Lavrentiev cruise 28 (1998) for support. We are grateful for technical and scientific support by Arne Sturm, Lester Lembke, Bastian Fessler, Stefan Müller, André Kaiser, Jutta Heinze (GEOMAR), Dirk Dethleff (IPÖ Kiel), Sergey Gorbarenko (V.I. Il'ichev Pacific Oceanological Institute, Far Branch of Russian Academy of Sciences, Vladivostok), Michael Levitan (Shirshow Institute of Oceanology, Moscow), and Yan Wen (Academia Sinica, Peking). Critical reviews of Zhongli Ding (Chinese Academy of Science, Beijing) and David Rea (University of Michigan, Ann Arbor) greatly improved the manuscript. AMS^{14}C measurements were kindly provided by the Leibniz Institut für Altersbestimmung, Univ. Kiel. Time series analyses were performed with AnalySeries 1.1 [*Paillard et al.*, 1996].

References

Alfutis, M. A., and S. Martin (1987), Satellite passive microwave studies of the Sea of Okhotsk ice cover and its relation to oceanic processes, 1978–1982, *J. Geophys. Res.*, *92*, 13,013–13,028.

Ananjev, G. S., E. G. Ananjeva, and A. J. Pakhomov (1984), Quaternary glaciation of the east Priokhotja, in *Pleistocene Glaciation of Eastern Asia*, edited by V. G. Bespaluj, pp. 43–56, Far Eastern Branch, Akad. Nauk SSSR, Magadan, Russia.

Ananjev, G. S., O. Y. Glushkova, and V. V. Kolpakova (1993), Stratigraphy and paleogeography of northeast Asia at Late Pleistocene, in *Evolution of Landscapes and Climate of the Northern Eurasia: Late Pleistocene-Holocene Elements of Prognosis*, edited by A. A. Velichko, pp. 59–61, Nauka, Moscow.

Anikiev, V. V., O. V. Dudarev, G. M. Kolesov, A. I. Botsul, and I. V. Utkin (2001), Factors of mesoscale variability in the distribution of the particulate matter and chemical elements in the Amur River estuary–Sea of Okhotsk waters, *Geochem. Int.*, *39*(1), 64–87.

Aota, M., and E. Uematsu (1989), The study on the polar ocean and the Sea of Okhotsk, *J. Geogr.*, *98*(5), 70–82.

Appollonio, S. (1973), Glaciers and nutrients in Arctic Seas, *Science*, *180*, 491–493.

Bassinot, F. C., L. D. Labeyrie, E. Vincent, X. Quidelleur, N. J. Shackleton, and Y. Lancelot (1994), The astronomical theory of climate and the age of the Brunhes-Matuyama magnetic reversal, *Earth Planet. Sci. Lett.*, *126*, 91–108.

Berger, A., and M. F. Loutre (1991), Insolation values for the climate of the last 10 million years, *Quat. Sci. Rev.*, *10*, 297–317.

Bezrukov, P. L. (1955), Distribution and accumulation rates opal sediments in the Okhotsk Sea (in Russian), *Dokl. Akad. Nauk SSSR*, *103*, 96–157.

Bezrukov, P. L. (1960), Bottom sediments of the Okhotsk Sea (in Russian), *Tr. Inst. Okeanol. im. P. P. Shirshova Akad. Nauk SSSR*, *32*, 96–157.

Biebow, N., and E. Hütten (1999), KOMEX cruise reports: KOMEX I and II: RV Professor Gagarinsky Cruise 22, RV Akademik M.A. Lavrentyev Cruise 28, *GEOMAR Rep*. *82*, 188 pp., Res. Cent. for Mar. Geosci. (GEOMAR), Kiel, Germany.

Biebow, N., et al. (2003), Cruise Reports: RV Akademik M.A. Lavrentyev Cruise 29, Leg 1 and Leg 2, *GEOMAR Rep*. *110*, Res. Cent. for Mar. Geosci. (GEOMAR), Kiel, Germany.

Boyle, E. A. (1988), Cadmium: Chemical tracer of deepwater paleoceanography, *Paleoceanography*, *3*(4), 471–489.

Braitseva, O. A., and I. V. Melekestsev (1974), Quaternary glaciation, in *Kamchatka*, *Kuril and Komandore Islands*, edited by I. B. Luchitskiy, pp. 426–438, Nauka, Moscow.

Cavalieri, D. J., and C. L. Parkinson (1987), On the relationship between atmospheric circulation and the fluctuations in the sea ice extents of the Bering and Okhotsk Seas, *J. Geophys. Res.*, *92*, 7141–7162.

COHMAP Members (1988), Climatic changes of the last 18,000 years: Observations and model simulations, *Science*, *241*, 1043–1052.

DeMaster, D. J. (1981), Measuring biogenic silica in marine sediments and suspended matter, in *Marine Particles: Analysis and Characterization*, *Geophys. Monogr. Ser.*, vol. 63, edited by D. C. Hurd and D. W. Spenser, pp. 363–368, AGU, Washington, D. C.

Ding, Z. L., T. S. Liu, N. W. Rutter, Z. W. Yu, T. Guo, and R. X. Zhu (1995), Ice-volume forcing of the east Asia winter monsoon variations in the past 80,0000 years, *Quat. Res.*, *44*, 149–159.

Ding, Z. L., E. Derbyshire, S. L. Yang, Z. W. Yu, S. F. Xiong, and T. S. Liu (2002), Stacked 2.6-Ma grain size record from the Chinese loess based on five sections and correlation with the deep-sea $\delta^{18}O$ record, *Paleoceanography*, *17*(3), 1033, doi:10.1029/2001PA000725.

Duce, R. A., and N. W. Tindale (1991), Atmospheric transport of iron and its deposition in the ocean, *Limnol. Oceanogr.*, *36*, 1715–1726.

Duce, R. A., et al. (1991), The atmospheric input of trace species to the world ocean, *Global Biogeochem. Cycles*, *5*(3), 193–259.

Emerson, S., and J. I. Hedges (1988), Processes controlling the organic carbon content of open ocean sediments, *Paleoceanography*, *3*, 621–634.

Engel, A. E. J., C. G. Engel, and R. G. Havens (1965), Chemical characteristics of ocean basalts and the upper Miocene, *Geol. Soc. Am. Bull.*, *76*, 719–734.

Freeland, H. J., A. S. Bychkov, F. Whitney, C. Taylor, C. S. Wong, and G. I. Yurasov (1998), WOCE section P1W in the Sea of Okhotsk: 1. Oceanographic data description, *J. Geophys. Res.*, *103*, 15,613–15,623.

Frenzel, B., M. Pesci, and A. A. Velichko (Eds.) (1992), *Atlas of Paleoclimates and Paleoenvironments of the Northern Hemisphere: Late Pleistocene–Holocene*, 153 pp., G. Fischer, New York.

Gao, Y., Y. J. Kaufman, D. Tanré, D. Kolber, and P. G. Falkowski (2001), Seasonal distributions of aeolian iron fluxes to the global ocean, *Geophys. Res. Lett.*, *28*(1), 29–32.

Gingele, F. X., M. Zabel, S. Kasten, W. J. Bonn, and C. C. Nürnberg (1999), Biogenic barium as a proxy for paleoproductivity: Methods and limitations of application, in *Use of Proxies in Paleoceanography*, edited by G. Fischer and G. Wefer, pp. 345–364, Springer-Verlag, New York.

Godbole, R. V., and J. Shukla (1981), Global analysis of January and July sea level pressure, *NASA Tech. Memo*, *82097*.

Goñi, M. A., K. C. Ruttenberg, and T. I. Eglington (1998), A reassessment of the sources and importance of land-derived organic matter in surface sediments from the Gulf of Mexico, *Geochim. Cosmochim. Acta*, *62*(18), 3055–3075.

Gorbarenko, S. A. (1996), Stable isotope and lithologic evidence of late-glacial and Holocene oceanography of the northwestern Pacific and its marginal seas, *Quat. Res.*, *46*, 230–250.

Gorbarenko, S. A., et al. (1988), Okhotsk Sea upper Quaternary sediment and reconstruction of paleoceanographic conditions (in Russian), *Pac. Ocean Geol.*, *2*, 25–30.

Gorbarenko, S. A., A. N. Derkachev, A. S. Astakhov, J. R. Sauton, D. Nürnberg, and V. V. Shapovalov-Chuprynin (2000a), Lithostratigraphy and tephrachronology of the Upper Quaternary deposits in the Sea of Okhotsk, *Geol. Pac. Ocean*, *19*(2), 58–82.

Gorbarenko, S. A., A. N. Derkachev, A. S. Astakhov, J. R. Southon, and D. Nürnberg (2000b), Lithostratigraphy and tephrachronology of the Upper Quaternary deposits in the Sea of Okhotsk, *Tikhookean. Geol.*, *19*(2), 58–72.

Gorbarenko, S. A., D. Nürnberg, A. N. Derkachev, A. S. Astakhov, J. R. Southon, and A. Kaiser (2002), Magnetostratigraphy and tephrachronology of the upper Quaternary sediments in the Okhotsk Sea: Implication of terrigenous, volcanogenic and biogenic matter supply, *Mar. Geol.*, *183*, 107–129.

Gorbarenko, S. A., V. Y. Leskov, A. V. Artemova, R. Tiedemann, N. Biebow, and D. Nürnberg (2003), Ice cover of the Sea of Okhotsk during the last glaciation and Holocene, *Dokl. Acad. Sci.*, *388*(5), 678–682.

Gromet, L. P., R. F. Dymek, L. A. Haskin, and R. L. Korotev (1984), The "North American shale composite": Its compilation, major and trace element characteristics, *Geochim. Cosmochim. Acta*, *48*, 2469–2482.

Harris, P. G., M. Zhao, A. Rosell-Melé, R. Tiedemann, M. Sarnthein, and J. R. Maxwell (1996), Chlorin accumulation rates as a proxy for Quaternary marine primary productivity, *Nature*, *383*, 63–65.

Heusser, L. E., and J. J. Morley (1985), Pollen and radiolarian records from deep-sea core RC14-103: Climatic reconstructions of the northeast Japan and northwest Pacific for the last 90,000 years, *Quat. Res.*, *24*, 60–72.

Holbourn, A., T. Kiefer, U. Pflaumann, and S. Rothe (2002), WEPAMA Cruise MD 122/IMAGES VII, *Rapp. Campagnes Mer OCE/2002/01*, Inst. Polaire Fr. Paul Emile Victor (IPEV), Plouzané, France.

Holeman, J. N. (1968), Sediment yield of major rivers in the world, *Water Resour. Res.*, *4*, 737–747.

Hovan, S. A., D. K. Rea, and N. G. Pisias (1991), Late Pleistocene continental climate and oceanic variability recorded in northwest Pacific sediments, *Paleoceanography*, *6*(3), 349–370.

Jacobs, S., A. L. Gordon, and A. F. Amos (1979), Effect of glacial ice melting on the Antarctic surface water, *Nature*, *277*, 469–471.

Jones, C. E., A. N. Halliday, D. K. Rea, and R. M. Owen (1994), Neodymium isotopic variations in North Pacific modern silicate sediment and the insignificance of detrital REE contributions to seawater, *Earth Planet. Sci. Lett.*, *127*, 55–66.

Jouse, A. (1962), *Stratigraphical and Paleogeographical Research in the Northwest Pacific (*in Russian), 258 pp., Akad. Nauk SSSR, Moscow.

Jouse, A., and E. V. Koreneva (1959), To the Okhotsk Sea paleogeography (in Russian), *Izv. Akad. Nauk, Ser. Geogr.*, *2*, 12–24.

Kaiser, A. (2000), Ozeanographie, Produktivität und Meereisverbreitung im Ochotskischen Meer während der letzten ca. 350 ka, Ph.D. thesis, Univ. Kiel, Kiel, Germany.

Keigwin, L. D. (1998), Glacial-age hydrography of the far northwest Pacific, *Paleoceanography*, *13*, 323–339.

Kent, D., N. D. Opdyke, and M. Ewing (1971), Climate change in the North Pacific using ice-rafted detritus as a climatic indicator, *Geol. Soc. Am. Bull.*, *82*, 2741–2754.

Kimura, N., and M. Wakatsuchi (2001), Mechanisms for the variation of sea ice extent in the Northern Hemisphere, *J. Geophys. Res.*, *106*, 31,319–31,332.

Kitani, K. (1973), An oceanographic study of the Okhotsk Sea—Particularly in regard to cold waters, *Bull. Far Seas Fish. Res. Lab.*, *9*, 45–75.

Koblentz-Mishke, O. J., V. V. Volkovinsky, and J. G. Kabanova (1970), Plankton primary production of the world ocean, in *Scientific*

Exploration of the South Pacific, edited by W. Wooster, pp. 183–193, Natl. Acad. of Sci., Washington, D. C.

Kowalik, Z., and I. Polyakov (1998), Tides in the Sea of Okhotsk, *J. Phys. Oceanogr.*, *28*(7), 1389–1409.

Kozdon, R. (2002), Kurzfristige Änderungen im Sedimentationsgeschehen des westlichen Ochotskischen Meeres während des Holozäns—Implikationen für den NE-sibirischen Raum, diploma thesis, 32 pp., Univ. Kiel, Kiel, Germany.

Krissek, L. (1995), Late Cenozoic ice-rafting records from Leg 145 sites in the North Pacific: Late Miocene onset, Late Pliocene intensification, and Pliocene-Pleistocene events, in *Proc. Ocean Drill. Proj. Sci. Results*, *145*, 3–19.

Leinen, M. (1989), The late Quaternary record of atmospheric transport to the northwest Pacific from Asia, in *Paleoclimatology and Paleometeorology: Modern and Past Patterns of Global Atmospheric Transport*, edited by M. Leinen and M. Sarnthein, pp. 693–732, Kluwer Acad., Norwell, Mass.

Lisitzin, A. (1951), Some data about coarse material distribution in the modern sea sediments (in Russian), *Dokl. Akad. Nauk SSSR*, *80*, 81–84.

Lisitzin, A. (1974), *Sedimentation in the Ocean* (in Russian), 438 pp., Nauka, Moscow.

Lutze, G. F., M. Sarnthein, B. Koopmann, and U. Pflaumann (1979), Meteor core 12309: Late Pleistocene reference section for interpretation of the Neogene of site 397, *Initial Rep. Deep Sea Drill. Proj.*, *47*, 727–739.

Mahowald, N., K. Kohfeld, M. Hansson, Y. Balkanski, S. P. Harrison, C. Prentice, M. Schulz, and H. Rohde (1999), Dust sources and deposition during the Last Glacial Maximum and current climate: A comparison of model results with paleodata from ice cores and marine sediments, *J. Geophys. Res.*, *104*, 15,895–15,916.

Mantua, N. J., S. R. Hare, Y. Zhang, J. M. Wallace, and R. C. Francis (1997), A Pacific interdecadal oscillation with impacts on salmon production, *Bull. Am. Meteorol. Soc.*, *78*, 1069–1079.

Martin, S., and M. Kawase (1998), The southern flux of sea ice in the Tatarskiy Strait, Japan Sea and the generation of the Liman Current, *J. Mar. Res.*, *56*, 141–155.

Matul, A., A. Abelmann, R. Tiedemann, A. Kaiser, and D. Nürnberg (2002), Late Quaternary polycystine radiolarian datum events in the Sea of Okhotsk, *Geo Mar. Lett.*, *22*, 25–32.

McLennan, S. (1995), Sediments and soils: Chemistry and abundances, in *Handbook of Physical Constants*, *Rock Physics and Phase Relations*, *Ref. Shelf Ser.*, vol. 3, pp. 8–19, AGU, Washington, D. C.

Milliman, J. D., and R. H. Meade (1983), Worldwide delivery of river sediment to the oceans, *J. Geol.*, *91*, 1–21.

Minobe, S. (1999), Resonance in bidecadal and pentadecadal climate oscillations over the North Pacific: Role in climate regime shifts, *Geophys. Res. Lett.*, *26*, 855–858.

Mix, A. C., N. G. Pisias, W. Rugh, J. Wilson, A. Morey, and T. H. Hagelberg (1995), Benthic foraminifer stable isotope record from Site 849 (0–5 Ma): Local and global climate changes, *Proc. Ocean Drill. Proj. Sci. Res.*, *138*, 371–412.

Miyazaki, S., and T. Yasunari (1999), Abrupt seasonal changes in surface climate observed in northern Mongolia by an automatic weather station, *J. Meteorol. Soc. Jpn.*, *77*, 583–593.

Müller, P. J. (1977), C/N ratios in Pacific deep-sea sediments: Effect of inorganic ammonium and organic nitrogen compounds sorbed by clays, *Geochim. Cosmochim. Acta*, *41*, 765–776.

Müller, P. J., and R. Schneider (1993), An automated leaching method for the determination of opal in sediments und particulate matter, *Deep Sea Res., Part I*, *40*(3), 425–444.

Narita, H., M. Sato, S. Tsunogai, M. Murayama, M. Ikehara, T. Nakatsuka, M. Wakatsuchi, N. Harada, and Y. Ujiié (2002), Biogenic opal indicating less productive northwestern North Pacific during the glacial ages, *Geophy. Res. Lett.*, *29*(15), 1732, doi:10.1029/2001GL014320.

Nimmergut, A., and A. Abelmann (2002), Spatial and seasonal changes of radiolarian standing stocks in the Sea of Okhotsk, *Deep Sea Res., Part I*, *49*, 463–493.

Nürnberg, C. C. (1995), Bariumfluss und Sedimentation im südlichen Südatlantik—Hinweise auf Produktivitätsänderungen im Quartär, *GEOMAR Rep. 38*, 105 pp., Res. Cent. for Mar. Geosci. (GEOMAR), Kiel, Germany.

Nürnberg, C. C., G. Bohrmann, M. Schlüter, and M. Frank (1997a), Barium accumulation in the Atlantic sector of the Southern Ocean: Results from 190,000-year records, *Paleoceanography*, *12*, 594–603.

Nürnberg, D., B. V. Baranov, and B. J. Karp (1997b), GREGORY cruise report: RV *Akademik M.A. Lavrentyev* Cruise 27, *GEOMAR Rep. 60*, 69 pp., Res. Cent. for Mar. Geosci. (GEOMAR), Kiel, Germany.

Nürnberg, D., R. Tiedemann, A. Kaiser, and N. Biebow (2003), Paleoceanographic studies in the Sea of Okhotsk—Implications for the glaciation history of NE Siberia, *Geophys. Res. Abstr.*, *5*, Abstract EAE03-A-11171.

Ogi, M., Y. Tchaibana, F. Nishio, and M. A. Danchenkov (2001), Does the fresh water supply from the Amur River flowing into the Sea of Okhotsk affect sea ice formation?, *J. Meteorol. Soc. Jpn.*, *79*, 123–129.

Ogi, T., K. Musiake, H. Matsuyama, and K. Masuda (1995), Global atmospheric water balance and runoff from large river basins, *Hydrol. Processes*, *9*, 655–678.

Ohtani, K., and Y. Nagata (1990), The role of the Okhotsk Sea on the formation of the Oyashio water, *Eos Trans. AGU*, *28*, 881.

Overland, J. E., J. Miletta Adams, and M. A. Bond (1999), Decadal variability of the Aleuten Low and its relation to high-latitude circulation, *J. Clim.*, *12*, 1542–1548.

Paillard, D., L. Labeyrie, and P. Yiou (1996), Macintosh program performs time-series analysis, *Eos Trans. AGU*, *77*, 379.

Parkinson, C. L. (1990), The impact of the Siberian High and Aleuten Low on the sea ice cover of the Sea of Okhotsk, *Ann. Glaciol.*, *14*, 226–229.

Parkinson, C. L., and A. J. Gratz (1983), On the seasonal sea ice cover of the Sea of Okhotsk, *J. Geophys. Res.*, *88*, 2793–2802.

Pfirman, S., M. A. Lange, I. Wollenburg, and P. Schlosser (1990), Sea ice characteristics and the role of sediment inclusions in deep-sea deposition: Arctic-Antarctic comparisons, in *Geological History of the Polar Oceans: Arctic versus Antarctic*, *NATO ASI Ser., Ser. C*, vol. 308, edited by U. Bleil and J. Thiede, pp. 187–212, Kluwer Acad., Norwell, Mass.

Pisias, N. G., and M. Leinen (1984), Milankovitch forcing of the oceanic system: Evidence from the northwest Pacific, in *Milankovitch and Climate: Understanding the Response to Astronomical Forcing*, *NATO ASI Ser., Ser. C*, vol. 126, part I, edited by A. L. Berger et al., pp. 307–330, Kluwer Acad., Norwell, Mass.

Ponomorev, V., O. Trusenkova, E. Ustinova, and D. Kaplunenko (1999), Interannual variations of oceanographic and meteorological characteristics in the Sea of Okhotsk, *PICES Sci. Rep.*, *12*, 31–40.

Prell, W. L., J. Imbrie, D. G. Martinson, J. J. Morley, N. G. Pisias, N. J. Shackleton, and H. F. Streeter (1986), Graphic correlation of oxygen isotope stratigraphy application to the Late Quaternary, *Paleoceanography*, *1*, 137–162.

Pye, K. (1987), *Aeolian Dust and Dust Deposits*, 334 pp., Academic, San Diego, Calif.

Rea, D. K. (1994), The paleoclimatic record provided by eolian deposition in the deep sea: The geologic history of wind, *Rev. Geophys.*, *32*(2), 159–195.

Redfield, A. C., B. H. Ketchum, and F. A. Richards (1963), The influence of organisms on the composition of seawater, in *The Sea*, vol. 2, edited by M. N. Hill, pp. 26–77, John Wiley, Hoboken, N. J.

Reynolds, R. L., and J. W. King (1995), Magnetic records of climate change, *U.S. Natl. Rep. Int. Union Geod. Geophys., 1991–1994*, *Rev. Geophys.*, *33*, 101–110.

Riser, S. C. (1990), Sources of North Pacific Intermediate Water from the Sea of Japan and Sea of Okhotsk, *Eos Trans. AGU*, *28*, 881.

Ronov, A. B., and A. A. Migdisov (1971), Geochemical history of the crystalline basement and sedimentary cover of the Russian and North American Platforms, *Sedimentology*, *16*, 137–185.

Rostov, I. D., and I. A. Zhabin (1991), Hydrological conditions of the Amur River near-mouth area (in Russian), *Meteorol. Gidrol.*, *7*, 94–99.

Saito, C., S. Noriki, and S. Tsunogai (1992), Particulate flux of Al, a component of land origin, in the western North Pacific, *Deep Sea Res., Part A*, *39*, 1315–1327.

Seki, O., K. Kawamura, T. Nakatsuka, K. Ohnishi, M. Ikehara, and M. Wakatsuchi (2003), Sediment core profiles of long-chain n-alkanes in the Sea of Okhotsk: Enhanced transport of terrestrial organic matter from the last deglaciation to the early Holocene, *Geophys. Res. Lett.*, *30*(1), 1001, doi:10.1029/2001GL014464.

Shackleton, N. J., and M. A. Hall (1984), Oxygen and carbon isotope stratigraphy of Deep Sea Drilling Project Hole 552A: Plio-Pleistocene glacial history, *Initial Rep. Deep Sea Drill. Proj.*, *81*, 599–609.

Shiga, K., and I. Koizumi (2000), Latest Quaternary oceanographic changes in the Okhotsk Sea based on diatom records, *Mar. Micropaleontol.*, *38*, 91–117.

Shimmield, G., S. Derrick, A. Mackensen, H. Grobe, and C. Pudsey (1994), The history of barium, biogenic silica and organic carbon accumulation in the Wedell Sea and Antarctic Ocean over the last 150,000 years, in *Carbon Cycling in the Glacial Ocean: Constraints on the Ocean's Role in Global Change*, *NATO ASI Ser., Ser. I*, vol. 17, edited by R. Zahn et al., pp. 555–574, Springer-Verlag, New York.

Skinner, L. C., and I. N. McCave (2003), Analysis and modelling of gravity- and piston cor-

ing based on soil mechanics, *Mar. Geol.*, *199*, 181–204.

Southon, J. R., D. E. Nelson, and J. S. Vogel (1990), A record of past ocean-atmosphere radiocarbon differences from the Northeast Pacific, *Paleoceanography*, *5*, 197–206.

St. John, K. E. K., and L. A. Krissek (1999), Regional patterns of Pleistocene ice-rafted debris flux in the North Pacific, *Paleoceanography*, *14*, 653–662.

Stuiver, M., and P. J. Reimer (1993), Extended ^{14}C data base and revised CALIB 3.0 ^{14}C age calibration program, in *Calibration 1993*, edited by M. Stuiver, A. Long, and R. S. Kra, *Radiocarbon*, *35*(1), 215–230.

Talley, L. D. (1991), An Okhotsk Sea water anomaly: Implications for ventilation in the North Pacific, *Deep Sea Res., Part A*, *38*, suppl. 1, 171–190.

Talley, L. D., and M. Y. Nagata (1995), *The Okhotsk Sea and Oyashio Region*, 227 pp., Inst. of Ocean Sci., Sidney, B. C., Canada.

Taylor, S. R., and S. M. McLennan (1981), The composition and evolution of the continental crust; rare earth element evidence from sedimentary rocks, *Philos. Trans. R. Soc. London, Ser. A*, *301*, 381–399.

Taylor, S. R., and S. M. McLennan (1985), *The Continental Crust: Its Composition and Evolution*, 312 pp., Blackwell, Malden, Mass.

Taylor, S. R., S. M. McLennan, and M. T. McCulloch (1983), Geochemistry of loess, continental crustal composition and crustal model ages, *Geochim. Cosmochim. Acta*, *47*, 1897–1905.

Tchaibana, Y., and G. Wakahama (1989), Effect of the equatorial Pacific Ocean on interannual variability in the Okhotsk sea ice, *Low Temp. Sci., Ser. A*, *48*, 71–77.

Tchaibana, Y., M. Honda, and K. Takeuchi (1996), The abrupt decrease of the sea ice over the southern part of the Sea of Okhotsk in 1989 and its relation to the recent weakening of the Aleutian Low, *J. Meteorol. Soc. Jpn.*, *74*, 579–584.

Ternois, Y., K. Kawamura, L. Keigwin, N. Ohkouchi, and T. Nakatsuka (2001), A biomarker approach for assessing marine and terrigenous inputs to the sediments of Sea of Okhotsk for the last 27,000 years, *Geochim. Cosmochim. Acta*, *65*(5), 701–802.

Thompson, P. R. (1981), Planktonic foraminifera in the western North Pacific during the past 150.000 years: Comparison on modern and fossil assemblages, *Palaeogeogr. Palaeoclimatol. Palaeoecol.*, *35*, 241–279.

Thompson, P. R., and N. J. Shackleton (1980), North Pacific palaeoceanography: Late Quaternary coiling variations of planktonic foraminifer *Neogloboquadrina pachyderma*, *Nature*, *287*, 829–833.

Tiedemann, R., and G. H. Haug (1995), Astronomical calibration of cycle stratigraphy for Site 882 in the northwest Pacific, in *Proc. Ocean Drill. Program Sci. Results*, *145*, 283–292.

Tiedemann, R., M. Sarnthein, and N. J. Shackleton (1994), Astronomic timescale for the Pliocene Atlantic $\delta^{18}O$ and dust flux records of Ocean Drilling Program Site 659, *Paleoceanography*, *9*, 619–638.

Trenberth, K. E., and J. W. Hurrell (1994), Decadal atmosphere ocean variations in the Pacific, *Clim. Dyn.*, *9*, 303–319.

Trenberth, K. E., G. W. Branstator, D. Karoly, A. Kumar, N.-C. Lau, and C. Ropelewski (1998), Progress during TOGA in understanding and modeling global teleconnections associated with tropical sea surface temperatures, *J. Geophys. Res.*, *103*, 14,291–14,324.

Ustinova, E. I., Y. D. Sorokin, and T. V. Dyomina (2000), Long-term variability of hydrometeorological parameters in the Japan, Okhotsk, and Bering Seas, in *Proceedings of CREAMS'2000, Oceanography of the Japan Sea*, edited by M. A. Danchenkov, pp. 230–240, Dalnauka, Vladivostok, Russia.

Van Andel, T. H., G. R. Heath, and T. C. Moore (1975), Cenozoic history and paleoceanography of the central equatorial Pacific, *Mem. Geol. Soc. Am.*, *143*, 134 pp.

Wadachi, K. (1987), *Encyclopedia of Oceanography*, 589 pp., Tokyodo, Tokyo.

Wakatsuchi, M., and S. Martin (1990), Satellite observations of the ice cover of the Kuril basin region of the Okhotsk Sea and its relation to the regional oceanography, *J. Geophys. Res.*, *95*, 13,393–13,410.

Wallace, J. M. (2000), North Atlantic Oscillation/Annular Mode: Two paradigms—One phenomenon, *Quat. J. R. Meteorol. Soc.*, *126*, 791–805.

Wang, L., M. Sarnthein, H. Erlenkeuser, J. Grimalt, P. Grootes, S. Heilig, E. Ivanova, M. Kienast, C. Pelejero, and U. Pflaumann (1999), East-Asian monsoon climate during the Late Pleistocene: High-resolution sediment records from the South China Sea, *Mar. Geol.*, *156*(1–4), 243–282.

Wang, W.-C., and K. Li (1990), Precipitation fluctuation over semi-arid region in northern China and the relationship with El Niño/Southern Oscillation, *J. Clim.*, *3*, 769–783.

Wedepohl, K. H. (1991), The composition of the upper Earth's crust in the natural cycles of selected metals: Metals in natural raw materials, in *Metals and Their Compounds in the Environment*, edited by E. Merian, chap. I.1, VCH, Weinheim, Germany.

Winckler, G., V. Sosnin, and A. Salyuk (1999), Hydrography of the Sea of Okhotsk, *GEOMAR Rep. 82*, Res. Cent. for Mar. Geosci. (GEOMAR), Kiel, Germany.

Wong, C. S., R. J. Matear, H. J. Freeland, F. A. Whitney, and A. S. Bychkov (1998), WOCE line P1W in the Sea of Okhotsk: 2. CFCs and the formation rate of intermediate water, *J. Geophys. Res.*, *103*, 15,625–15,642.

Yoneda, M., H. Kitagawa, J. van der Plicht, M. Uchida, A. Tanaka, T. Uehiro, Y. Shibata, M. Morita, and T. Ohno (2000), Pre-bomb marine reservoir ages in the western North Pacific: Preliminary results on Kyoto University collection, *Nucl. Instrum. Methods, Sect. B*, *172*, 377–381.

Zech, W., R. Bäumler, O. Savoskul, and G. Sauer (1996), Zur Problematik der pleistozänen und holozänen Vergletscherung Süd-Kamtschatkas—erste Ergebnisse bodengeographischer Untersuchungen, *Eiszeitalter Ggw.*, *46*, 132–143.

Zech, W., R. Bäumler, O. Savoskul, O. A. Braitseva, and J. Melekestsev (1997), Evidence of Middle Pleistocene glaciation in SW-Kamtchatka, *Z. Gletscherkd. Glazialgeol.*, *33(1), 15–20.*

Zenkevitch, L. (1963), *Biology of the Seas of the U.S.S.R*, Wiley-Interscience, Hoboken, N. J.

D. Nürnberg and R. Tiedemann, Leibniz Institut für Meereswissenschaften, Wischhofstrasse 1-3, D-24148 Kiel, Germany. (dnuernberg@ifm-geomar.de; rtiedemann@ifm-geomar.de)